Inflammasome in respiratory epithelial cells restricts influenza virus infection

インフルエンザウイルス感染抑制に関与する気道上皮由来インフラマソーム活性化機構の解析

2018

筑波大学グローバル教育院

School of Integrative and Global Majors in University of Tsukuba

Ph.D. program in Human Biology

SangJoon Lee

筑　波　大　学

University of Tsukuba

博士（人間生物学）学位論文

Ph.D. dissertation in Human Biology

Inflammasome in respiratory epithelial cells restricts influenza virus infection

インフルエンザウイルス感染抑制に関与する気道上皮由来インフラマソーム活性化機構の解析

2018

筑波大学グローバル教育院

School of Integrative and Global Majors in University of Tsukuba

Ph.D. program in Human Biology

SangJoon Lee

Table of Contents

Chapter I. Introduction

1. General remarks of influenza A virus

1-1 Influenza A virus genome and viral proteins

Influenza A virus (IAV) is a member of the family *Orthomyxoviridae*. The genome of IAV consists of a set of eight-segmented ssRNAs of negative polarity, and is complexed with the viral RNA polymerase and nucleoprotein (NP) in virion (Fig. 1). The RNA polymerase is composed of three subunits, PB1, PB2, and PA encoded in three largest RNA segments. NP is an RNA binding protein encoded by the RNA segment 5. Infection of IAV occurs via interaction between its surface glycoprotein, hemagglutinin (HA) and sialic acids on the surface of host cell membrane. HA is a type I transmembrane protein encoded by the RNA segment 4. The other glycoprotein, neuraminidase (NA) is a type II transmembrane protein encoded by the RNA segment 6. It has been widely accepted that HA and NA are essential for virus entry and budding process, respectively (1, 2). Matrix protein 1 (M1) encoded by the RNA segment 7 is the most abundant structural protein in virions (3). The RNA segment 7 also encodes for M2 via alternative splicing and M2 functions as an ion channel. The RNA segment 8 codes for nonstructural protein 1 (NS1) and NS2, the latter of which is generated through splicing of NS1 mRNA. NS1 is a multi-functional RNA binding protein and an important regulator of host immune responses and apoptotic cell death. NS2 mediates the nuclear export of virion RNAs by acting as an adaptor between viral ribonucleoprotein complexes and the nuclear export machinery of the cell. The infecting RNP is transported into nucleus, where transcription and replication of IAV occurs, followed by progeny RNP production.

Progeny RNP is then exported from nucleus to cytoplasm where virus assembly takes place.

1-2 IAV pathogenesis and history of IAV pandemics

IAV can infect diverse host species including pigs, birds, and humans. Human infection by IAV initiates in the respiratory tract and the virus induces inflammatory responses as a result of respiratory epithelial cell death (4, 5). The pro-inflammatory response from respiratory epithelial cells triggers migration of immune cells including macrophages and neutrophils to remove infectious agents. These migrated immune cells contribute to further inflammation (Fig. 2).

Through human history, IAV caused epidemics and severe pandemics at several times. In 1918, Spanish IAV, which killed 40-50 million people, is the first of the two pandemics involving H1N1 IAV (the second being the 2009 influenza pandemic) (6). Furthermore, in 1957-1958 and 2009, two IAV pandemics spread in southern China killed about 4 million people (7), and also a recent outbreak of human infections with a new avian IAV (H7N9), which caused 132 patients, including 37 deaths in 2013 (8).

1-3 Significance of IAV research

Seasonal IAV infections in humans cause annual epidemics, leading to millions of human infections worldwide and having significant health and economic burdens; IAV pandemics can also have devastating effects globally, resulting in millions of deaths. Within one year, this virus spread to all the world and caused > 18,000 confirmed deaths (9). Thus, IAV research plays an important role for

protection of public health as well as economic developments globally. Also it would be important to develop new vaccines and anti-influenza drugs.

2. General remarks of inflammation

2-1 Overview of the inflammatory response

Inflammation is an adaptive response that is triggered by noxious stimuli, infection, and tissue injury. The acute inflammatory response triggered by infection or tissue injury stimulates to recruit plasma and leukocytes to the site of infection or injury. The initial infection is recognized by Toll-like receptors (TLRs) and NOD-like receptors (NLRs), leading to the production of a variety of inflammatory mediators, including chemokines, cytokines, vasoactive amines, eicosanoids and products of proteolytic cascades (10). The main immediate effect of these mediators is to elicit an inflammatory exudate locally so that plasma proteins and leukocytes gain access to the blood vessels through the postcapillary venules. The activated endothelium of the blood vessels allows selective extravasation of neutrophils while preventing the exit of erythrocytes. When neutrophils reach the afflicted tissue site, the neutrophils become activated either by direct contact with pathogens or through the actions of cytokines secreted by tissue-resident cells. The neutrophils attempt to kill the invading pathogens by releasing the toxic contents of their granules, which include reactive oxygen species (ROS) and reactive nitrogen species, proteinase 3, cathepsin G and elastase (11). These potent effectors do not discriminate between microbial and host targets, so collateral damage to host tissues is unavoidable (12).

A successful acute inflammatory response results in the elimination of the infectious agents followed by a resolution and repair phases, which is mediated by tissue-resident and recruited macrophages (13). The switch in lipid mediators from pro-inflammatory prostaglandins to lipoxins, which are anti-inflammatory, is crucial for the transition from inflammation to resolution. Lipoxins inhibit the recruitment of

neutrophils, but promote the recruitment of monocytes, which remove dead cells and initiate tissue remodeling (13). If the acute inflammatory response fails to eliminate pathogens, the neutrophil infiltrate is replaced with macrophages and a chronic inflammatory state ensues with the formation of granulomas and tertiary lymphoid tissues (14).

2-2 Inducers of inflammation

Exogenous inducers can be classified into two groups: microbial and non-microbial. Pathogen-associated molecular patterns (PAMPs) are a major microbial inducers carried by all microorganisms (15). PAMPs are recognized by pathogen recognition receptors (PRRs) including TLRs and NLRs. Non-microbial exogenous inducers of inflammation include allergens, irritants, foreign bodies and toxic compounds (16).

Endogenous inducers of inflammation are signals produced by stressed, damaged tissues. One common theme in detecting acute tissue injury is the sensing of the desequestration of cells or molecules that are normally kept separate in intact cells and tissues (16).

2-3 Mediators of inflammation

Inducers trigger inflammatory processes through the release of inflammatory mediators, cytokines and chemokines. The cytokines including (tumor-necrosis factor-α (TNF-α) and interleukin-1 (IL-1)) have autocrine and paracrine effects leading to the local activation of macrophages and neutrophils, but when these cytokines are released in large amounts, they can exert endocrine effects, such as induction of platelet activation, fever, fatigue, and anorexia (17). The main function

of chemokines is to recruit additional immune cells to the site of infection. These immune cells include neutrophils, which exert a role in the phagocytosis and killing of pathogens (18, 19).

In the bloodstream, activated monocytes and neutrophils release cytokines, which stimulate the release of prostaglandins, molecules that mediate the signs and symptoms of illness (somnolence, fatigue, and fever) by acting on the hypothalamus (20). An important aspect of mediators of inflammation in the circulation is the activation of the complement system, which mediates microbial opsonization and killing, and generates inflammatory peptides such as C3a and C5a (21).

2-4 Effects of inflammation

Although the most obvious effect of inflammatory mediators is to induce the formation of an exudate, many inflammatory mediators also have effects on maintenance of tissue homeostasis (22). These functions of inflammatory mediators reflect a more general role for inflammation in the control of tissue homeostasis and in adaptation to noxious conditions.

3. Purpose and summary of this study

Respiratory epithelium functions as a sensor of infectious agents to initiate inflammatory responses along with cell death. However, the exact cell death mechanism responsible for inflammatory responses to IAV infection is still unclear. I found that IAV infection induced apoptosis or pyroptosis in both normal and precancerous human bronchial epithelial cells. Pyroptosis is a caspase-1-dependent inflammatory cell death controlled by inflammasomes, multiprotein complexes consisting of caspase-1, apoptosis-associated speck like protein containing a CARD (ASC), and cytoplasmic PRRs such as NLR family proteins. NLR family PYD-containing 3 (NLRP3) has been extensively characterized in monocytes and macrophages against IAV infection. However, the exact mechanism of inflammasome activation in respiratory epithelial cells, especially a sensor molecule for IAV infection, is largely unknown. To identify a novel respiratory epithelium-specific inflammasome receptor, I performed a high-content shRNA library screening and a proteomic analysis of ASC interacting proteins upon IAV infection. Using these two screening systems, I identified a human myxovirus resistance gene 1 (MxA) as a novel inflammasome receptor in respiratory epithelial cells that specifically forms inflammasome complexes with ASC and caspase-1 to promote proteolytic activation of IL-1β and IL-18. My study highlights the significance of epithelial inflammatory response mediated by MxA inflammasome, and human Mx-transgenic mice can be a valuable animal model for human respiratory epithelium to demonstrate inflammatory response upon virus infection.

4. Abbreviations

AAH	atypical adenomatous hyperplasia
ASC	apoptosis-associated speck like protein containing a CARD
ADV	adenovirus
AIM2	absent in melanoma 2
BAL	bronchoalveolar lavage
CARD	caspase recruitment domain
DAMPs	damage-associated molecular patterns
GBPs	guanylate-binding proteins
HA	hemagglutinin
hMx-Tg	human MxA transgenic
IAV	influenza A virus
IFI16	interferon gamma inducible protein 16
IFN	interferon
IL-1	interleukin-1
ISGs	interferon-stimulated genes
M1	matrix protein 1
MxA	myxovirus resistance gene 1
MOI	multiplicity of infection
NA	neuraminidase
NHBE	primary normal human bronchial epithelial cells
NLR	NOD-like receptor
NLRC4	NLR family CARD domain containing 4
NLRP3	NLR family PYD-containing 3

NP	nucleoprotein
NS1	nonstructural protein 1
PA	polymerase acidic protein
PAMPs	pathogen-associated molecular patterns
PB1	polymerase basic protein 1
PB2	polymerase basic protein 2
PBMC	primary human peripheral blood mononuclear cells
PRRs	pathogen recognition receptors
PYD	pyrin domain
RIP1	receptor interacting protein 1
ROS	reactive oxygen species
SeV	sendai virus
TLRs	toll-like receptors
TNF-α	tumor-necrosis factor-α
vRNP	viral ribonucleoprotein

Chapter II. Influenza A virus infection triggers pyroptosis and apoptosis of respiratory epithelial cells through type I IFN signaling pathway in a mutually exclusive manner

1. Introduction

1-1 Programmed cell death pathways

Various pathogens cause mainly three programmed cell death pathways, apoptosis, necroptosis, and pyroptosis (23-25). Apoptosis is a caspase-3-dependent cell death, and apoptotic cells are rapidly phagocytized and cleared without inflammatory responses (26). Necroptosis is a receptor interacting protein 1 (RIP1) and RIP3 kinases complex-dependent but caspase-independent inflammatory cell death by releasing damage-associated molecular patterns (DAMPs) (27). Pyroptosis is a caspase-1-dependent inflammatory cell death controlled by inflammasomes, multiprotein complexes consisting of caspase-1, ASC, and PRRs such as NLR family proteins. The formation of inflammasomes induced by virus infection is mainly observed in immune cells and results in the extracellular release of pro-inflammatory cytokines, such as IL-1β and IL-18 (28, 29) (Fig. 3).

1-2 Significant impacts of respiratory epithelial cells against IAV infection

The epithelial surface of lungs are in direct contact with the environment and are involved in physical segregation of hosts from a vast array of antigens, pollutions, and infectious agents. The respiratory epithelial cells also function as a sensor of

infectious agents to initiate inflammatory responses along with cell death by infection (30).

IAV stimulates inflammatory responses as a result of respiratory epithelial cell death (4, 5). The pro-inflammatory response from respiratory epithelial cells triggers recruitment of leukocytes including macrophages and neutrophils to remove infectious agents. These migrated immune cells contribute to excessive inflammation. Thus, the inflammatory response mechanism of the respiratory epithelium is crucial for understanding the pathogenesis of IAV. However, it has been reported that apoptosis is a major cell death pathway triggered by IAV infection in cultured epithelial cells isolated from malignant tumors (31-33). Therefore, the exact cell death mechanism responsible for inflammatory responses, which may determine the pathogenesis of IAV, is still unclear.

1-3 Cross talk of cell death pathways

Emerging evidence has shown the crosstalk of programmed cell death pathways (26), but the molecular mechanism to determine one of the cell death pathways remains poorly understood. Necroptosis is induced by several stimuli, which can also trigger apoptosis, in the presence of caspase inhibitors. Because, caspase-8 activated by apoptotic stimuli suppresses necroptosis by cleaving substrates such as RIP1 and RIP3 kinases (34, 35). Although endogenous inhibitors of caspase-8 to induce necroptosis are not understood, virally encoded caspase inhibitors are well-known examples to promote necroptosis (27). Therefore, necroptosis could be evolved as a host backup system to trigger cell death in virus-infected cells. It is well-known that mitochondria release several pro-apoptotic proteins including cytochrome C, through mitochondrial dysfunction. Dysfunctional mitochondria also activate

inflammasome assembly through mitochondrial ROS (36), released mitochondrial DNA (37, 38), and cardiolipin (39), but the exact role of mitochondria in pyroptosis activation remains controversial (40). It is reported that MAVS, which is an adapter molecule to transduce interferon (IFN) signaling pathway triggered by a viral RNA sensor RIG-I, interacts with NLRP3 and stimulates inflammasome formation (41, 42). Although it is reported that RIG-I activates inflammasome through a type I IFN-positive feedback loop in respiratory epithelial cells (43), type I IFN has been shown to negatively regulate the inflammasome formation in macrophages (44). Thus, despite considerable progress in understanding each cell death pathway, it remains controversial how viruses induce each cell death possibly due to the differences of stimuli and cell types used.

2. Materials and methods

2-1 Reagents

Mouse monoclonal antibody against ASC (Millipore), β-Actin (SIGMA), caspase-1 (R&D systems), GSDMDC1 (Santa Cruz Biotechnology), and rabbit polyclonal antibodies against cleaved caspase-3 (Cell Signaling Technology), pro-caspase-3 (Cell Signaling Technology), STAT1 α/β (Santa Cruz Biotechnology), phospho-(Tyr701) STAT1 (Cell Signaling Technology) were purchased. Z-DEVD-FMK (R&D systems), VX-765 (Chemietek), GSK-872 (Millipore), Z-VAD-FMK (Enzo Life Science), camptothecin (Calbiochem), IFN-β (Toray), ruxolitinib (Cayman) were purchased.

2-2 Cell culture and viruses

PL16B and PL16T cells were grown in MCDB153HAA with 0.5 ng/ml epidermal growth factor, 5 μg/ml insulin, 72 ng/ml hydrocortisone, 10 μg/ml transferrin, 20 ng/ml sodium selenium, and 2% fetal bovine serum (45). PC9, H1650, HCC827 cells were grown in Roswell Park Memorial Institute medium (RPMI) 1640 with 10% fetal bovine serum. H1975 cells were grown in RPMI 1640 containing high glucose with 10% fetal bovine serum. NHBE cells were purchased and the cells were grown in B-ALI^{TM} Growth Medium (Lonza). A549 cells were grown in Dulbecco's modified essential medium (DMEM) containing 10% fetal bovine serum. Influenza virus A/Puerto Rico/8/34 strain and human adenovirus type 5 (HAdV5) were prepared as previously described (46). R38A/K41A and Y89F mutant viruses (A/Puerto Rico/8/34 genetic backbone) were constructed as previously described (47, 48). del

NS1 virus was a generous gift from Dr. Adolfo Garcia-Sastre (Icahn School of Medicine at Mount Sinai).

2-3 Trypan blue dye exclusion assay

After pre-treatment of cells with each cell death inhibitor for 1 h, the cells were infected with IAV at a multiplicity of infection (MOI) of 10. At the indicated time points, both adherent and floating cells were collected and resuspended in 0.02% trypan blue (SIGMA) in phosphate-buffered saline (PBS). The number of dead and living cells was counted using hemocytometer.

2-4 DNA fragmentation assay

PL16T cells (5×10^3 cells) seeded in 96-well optical bottom plate (Thermo) and the cells were infected with IAV at a MOI of 10. At the indicated time points, the cells were stained with Hoechst 33342 and the number of DNA fragmented cells was quantified by ArrayScan^{TM} high-content systems (Thermo).

2-5 Indirect immunofluorescence assays

Cells were fixed with 3% paraformaldehyde (PFA) for 10 min and permeabilized with 0.5% Triton X-100 in PBS containing 0.2% bovine serum albumin (BSA) for 3 min. After incubation in PBS containing 1% skim milk for 1 h, the cells were incubated with primary antibodies for 1 h. After a washing with PBS containing 0.1% Tween 20 and 0.2% BSA, the cells were incubated with either Alexa Fluor 488- or 568-conjugated secondary antibodies, respectively (Invitrogen) for 30 min. Images were acquired by confocal laser scanning microscopy (LSM700; Carl Zeiss) using × 63 Apochromat objective.

2-6 Quantitative real-time PCR

Total RNA was isolated from PL16T cells by the acid guanidinium phenol chloroform method. cDNA was prepared from purified RNA (1 μg) by using ReverTraAce (Toyobo) with oligo $(dT)_{20}$ primer. Real-time PCR was carried out using SYBR Green Realtime PCR Master Mix-Plus (Roche) in the Thermal Cycler Dice Real-Time PCR system (TaKaRa).

Primer sequences

Bcl-xL Forward	5′-GCCACTTACCTGAATGACCAC-3′
Bcl-xL Reverse	5′-TGCTGCATTGTTCCCATAGA-3′
IFN-β Forward	5′-TGCCTCAAGGACAGGATGAAC-3′
IFN-β Reverse	5′-GCGTCCTCCTTCTGGAACTG-3′
18S rRNA Forward	5′-AACGGCTACCACATCCAAGG-3′
18S rRNA Reverse	5′-GGGAGTGGGTAATTTGCGC-3′

2-7 Cytokine measurements

Cytokines were measured by ELISA with human IL-1β (R&D system) according to the manufacturers' instruction.

2-8 Statistical analysis

Statistical significance was tested using a two-tailed Student's t-test. n/s, not significant. ***$P < 0.001$, **$P < 0.01$.

3. Results

3-1 Precancerous respiratory epithelial cells induce pyroptotic cell death in response to infection

To determine whether respiratory epithelial cell lines are susceptible to the cell death induced by IAV infection, I carried out trypan blue dye exclusion assays at 24 h post infection with different types of human malignant tumor respiratory epithelial cells (A549, PC9, H1975, H1650, and HCC827), human atypical adenomatous hyperplasia (AAH) respiratory epithelial cells (PL16T), human non-neoplastic respiratory epithelial cells (PL16B), and primary normal human bronchial epithelial cells (NHBE). Cell death in all malignant tumor cell lines was rarely induced by IAV infection, whereas the number of dead cells in PL16T, PL16B, and NHBE cells was 30 to 40% of total cells at 24 h post infection, respectively (Fig. 4). PL16T is an immortalized cell line, established from a precancerous region of lung adenocarcinoma patient (45). It has been reported that PL16T cells do not have any tumorigenic activity and there is no mutations or abnormal expressions of oncogenesis-related genes such as p53, Akt, and EGFR (49). To determine what kinds of cell death pathways are activated by IAV infection, I treated infected PL16T, NHBE, and A549 cells with each type of cell death inhibitor; Z-DEVD-FMK (caspase-3 inhibitor, Fig. 5A, C, E, and G), VX-765 (caspase-1 inhibitor, Fig. 5B, D, F, and H), and GSK-872 (RIP3 inhibitor, Fig. 5I, J, and K). In infected PL16T cells, the number of dead cells either stained with trypan blue dye (Fig. 5A) or having fragmented DNA (Fig. 5C) was reduced by the addition of the caspase-3 inhibitor at 12 and 24 h post infection, but not after 36 h post infection. In contrast, the caspase-1 inhibitor repressed the cell death even at 36 h post infection in infected PL16T cells

(Fig. 5B and D). These results suggest that apoptosis is induced in infected PL16T cells at early phases of infection, but the cell death pathway is shifted to pyroptosis at late phases of infection. Similar cell death results were obtained with infected NHBE cells (Fig. 5E and F). Furthermore, the number of dead cells in infected A549 cells decreased by the caspase-3 inhibitor in both early and late phases of infection, but not by the caspase-1 inhibitor (Fig. 5G and H). Thus, it is likely that IAV infection triggers both apoptotic and pyroptotic cell deaths in precancerous or normal human respiratory epithelial cells, but only apoptotic cell death in malignant tumor cells. GSK-872 did not inhibit cell death by IAV infection in PL16T cells, NHBE cells, and A549 cells (Fig. 5I, J, and K). These results indicate that necroptosis merely occurs in response to IAV infection in cultured cells I used. Note that the expression level of viral protein NP in PL16T cells was similar to that in A549 cells, indicating that the virus infectivity was comparable between A549 cells and PL16T cells (Fig. 5L).

3-2 IAV infection induces inflammasome assembly and IL-1β secretion in human respiratory epithelial cells

Upon inflammasome formation, ASC is assembled into a micrometer-sized perinuclear structure called an ASC speck to recruit procaspase-1 for its proteolytic self-activation. Then, the activated caspase-1 cleaves several substrates such as gasdermin D for pyroptosis induction, and also activates the secretion of inflammatory cytokines, IL-1β and IL-18, by digestion of their immature forms (50). Inflammasomes have been extensively characterized in monocytes and macrophages but not respiratory epithelial cells, although the epithelial cells may play an important role in early host immune response to infection. To confirm whether apoptosis and pyroptosis are induced in PL16T cells by IAV infection, I examined the proteolytic

activation of caspase-3 (Fig. 6A), caspase-1 (Fig. 6B), and gasdermin D (Fig. 6C) respectively. The cell lysates prepared from infected cells at 24 (Fig. 6A) and 48 h post infection (Fig. 6B and C) were subjected to western blotting analyses with anti-procaspase-3, anti-cleaved caspase-3, anti-caspase-1, and anti-gasdermin D antibodies. Camptothecin (CPT), a potent inhibitor of DNA topoisomerase-I, was used as a positive control for apoptosis induction (Fig. 6A, lane 3). Caspase-3, caspase-1, and gasdermin D were cleaved in IAV-infected PL16T cells (Fig. 6A, lane 7; B, lane 6; C, lane 2), but not when caspase-3 and caspase-1 inhibitors were added (Fig. 6A, lanes 4−6; B, lanes 3−5; C, lane 3).

To examine whether inflammasomes are formed, I carried out indirect immunofluorescence assays with anti-ASC antibody in PL16T, NHBE, and A549 cells. At 48 h post infection, ASC specks were observed in approximately 30% of total PL16T and NHBE cells, but not in A549 cells (Fig. 7A). I next examined IL-1β secretion from PL16T, NHBE, and A549 cells in response to IAV infection by enzyme-linked immunosorbent assays (ELISA). At 72 h post infection, approximately 50 pg/ml of IL-1β was secreted from infected PL16T and NHBE cells, however, I could not detect IL-1β secretion from infected A549 cells (Fig. 7B).

3-3 Apoptosis and pyroptosis are independently induced by IAV infection in respiratory epithelial cells

Next, I examined the number of apoptotic and pyroptotic cells by indirect immunofluorescence assays with anti-cleaved caspase-3 and anti-ASC antibodies to distinguish each cell death pathway. About 35% of infected cells was stained with anti-cleaved caspase-3 antibody at 24 h post infection, and the signals were reduced at 36 h post infection along with the apoptotic cell fragmentation (Fig. 8A). In contrast,

the number of ASC speck-positive cells was peaked at 48 h post infection (Fig. 8B). Further, both activated caspase-3- and ASC speck-positive cells were hardly observed (Fig. 8C and D), suggesting that apoptosis and pyroptosis are independently induced by IAV infection in PL16T cells.

3-4 Type I IFN-mediated JAK-STAT signaling pathway promotes the switch from apoptosis to pyroptosis by inhibiting apoptosis possibly through the induced expression of *Bcl-xL* anti-apoptotic gene

The viral nonstructural protein 1 (NS1) is a multi-functional RNA binding protein, and is known to be an important regulator of host immune responses and apoptotic cell death. NS1 inhibits dsRNA-mediated PKR activation and IFN-β production through its RNA binding activity (51). Also, NS1 prevents IFN-β production by inhibiting the activation of RIG-I through the interaction with TRIM25 (52). NS1 activates PI3K signaling by binding to the p85β regulatory subunit of PI3K (47). This results in the activation of Akt kinase, and the activated Akt protein phosphorylates proapoptotic Bcl-2 family proteins to inhibit apoptosis. I next examined the number of apoptotic and pyroptotic cells triggered by IAV NS1 mutants listed below: R38A/K41A mutant which is deficient in dsRNA-binding activity and in IFN antagonism (51); Y89F mutant which is deficient in PI3K/Akt activation for the inhibition of proapoptotic proteins (47); and del NS1 mutant which contains a deletion of *NS1* gene (53) (Fig. 9). I found that R38A/K41A mutation increased the inflammasome formation, but not the cleavage of procaspase-3, more than 5 times compared to WT at 24 h post infection (Fig. 9), suggesting that enhanced type I IFN production increases pyroptotic cell death upon IAV infection. In contrast, Y89F mutation increased apoptosis, but not pyroptosis, possibly due to the inability to

inhibit proapoptotic Bcl-2 family proteins including BAD (Fig. 9). I also found that del NS1 virus infection stimulated pyroptosis, but not apoptosis, consistent to R38A/K41A mutant virus. This suggests that type I IFN signaling pathway may antagonize proapoptotic Bcl-2 family proteins for the mutually exclusive activation of apoptosis and pyroptosis. Note that *IFN-β* gene was transcribed in wild-type IAV-infected PL16T cells at 48 h post infection, although the response was not quick possibly due to the inhibition by NS1 (Fig. 10A). The Bcl-2 family proapoptotic BH3 only protein BAD interacts with Bcl-xL anti-apoptotic protein to release apoptogenic factors such as cytochrome c from mitochondria to induce apoptosis. Akt kinase phosphorylates BAD, which is retained in the cytoplasm through the interaction with 14-3-3 proteins to prevent heterodimerization with Bcl-xL at the mitochondrial membrane (54, 55). It has been known that the expression level of Bcl-xL, but not Bcl-2, is regulated through STAT5, Ets, Rel/NF-kB, and AP-1 transcription factors in response to survival signaling pathways (56), although the effect of IAV infection on Bcl-xL expression is still unclear. To address this, I examined the amount of *Bcl-xL* mRNA in infected PL16T cells in the absence or presence of 1 μg/ml ruxolitinib, a potent inhibitor of JAK-STAT signaling pathway, which is a downstream of type I IFN receptor. The level of *Bcl-xL* mRNA was increased about three times by IAV infection in PL16T cells, and this increase was significantly repressed by ruxolitinib treatment (Fig. 10B). Therefore, it is possible that the induced expression of Bcl-xL by JAK-STAT pathway antagonizes proapoptotic Bcl-2 family proteins to inhibit the apoptotic cell death in infected PL16T cells.

3-5 Type I IFN signaling pathway triggers pyroptosis but represses apoptosis in a mutually exclusive manner

To elucidate whether type I IFN production is involved in the mutually exclusive activation of apoptosis and pyroptosis in IAV-infected PL16T cells, I examined the phosphorylation level of STAT1, which is a downstream transcription factor of type I IFN receptor. The phosphorylation level of STAT1 increased at 36 h post infection concomitant with pyroptosis activation (Fig. 11A and 8B). Further, I treated infected PL16T and NHBE cells with 1 μg/ml ruxolitinib and performed the indirect immunofluorescence assays using anti-ASC and anti-cleaved caspase-3 antibodies (Fig. 11B and C). By the addition of ruxolitinib, the number of ASC speck-positive cells decreased to approximately 30% of that in the absence of ruxolitinib (Fig. 11B). In contrast, the number of cleaved caspase-3-positive cells was increased more than 3 times by ruxolitinib treatment at 48 h post infection (Fig. 11C). Next, to examine the effect of type I IFN on the pyroptosis induction, infected cells were treated with 1,000 IU/ml IFN-β at 6 h post infection, at which viral proteins are fully expressed while apoptosis is not activated (Fig. 5A and L). At 24 h post infection, I carried out the indirect immunofluorescence assays using anti-ASC and anti-cleaved caspase-3 antibodies (Fig. 12A and B). Approximately 10% of PL16T cells showed ASC specks at 24 h post infection in the absence of IFN-β, and the number of ASC speck-positive cells increased to more than 50% by IFN-β treatment (Fig. 12A). In contrast, the number of cleaved caspase-3-positive cells was reduced in infected PL16T cells in the presence of IFN-β (Fig. 12B). I could not detect cells with ASC speck and cleaved caspase-3 (Fig. 12C). These findings suggest that type I IFN signaling pathway is responsible for switching cell death pathway from apoptosis to pyroptosis in infected respiratory epithelial cells. Note that there were no detectable ASC speck-positive A549 cells even in the presence of IFN-β (Fig. 12D),

suggesting that type I IFN production is not sufficient to induce pyroptosis in malignant tumor cells in response to IAV infection.

4. Discussion

Respiratory epithelium functions as a sensor of infectious agents to initiate inflammatory responses along with cell death. However, the exact cell death mechanism responsible for inflammatory responses to IAV infection is still unclear. In this study, IAV infection induced apoptosis and pyroptosis in normal or precancerous human bronchial epithelial cells, but it did not induce pyroptosis in malignant tumor respiratory epithelial cells (Fig. 4, 5, and 7). It has been reported that along with the establishment of malignancy in the tumor microenvironment, genetic mutations and epigenetic modifications are induced leading to abnormal expression of genes related to cell death and cell survival such as p53 and Akt (57, 58). Tissue homeostasis could be disorganized during carcinogenesis and could lead to inflammatory responses to recruit immune cells at the tumor microenvironment to eliminate the tumor cells (59). Thus, only immunosilent tumor variants would develop into malignant tumor cells, suggesting that signaling pathways to trigger pyroptosis may be declined along with the tumor development, thereby allowing cells to escape from cancer immunosurveillance.

My studies also highlight that necroptosis merely occurs in response to IAV infection in cultured cells I used. However, it has been reported that necroptosis is triggered by IAV infection in a mouse model (60) and immortalized murine cells including lung epithelial cells and embryonic fibroblast cells (61). Thus, it is possible that necroptosis is stimulated by IAV infection in a species- and/or cell type-dependent manner as previously reported in other virus infection such as herpes simplex virus (62), human cytomegalovirus (63), and human immunodeficiency virus (64).

I demonstrated that apoptosis is induced at early phases of infection, but the cell death pathway is shifted to pyroptosis at late phases of infection under the regulation of type I IFN signaling to promote pro-inflammatory cytokines production (Fig. 13). The cytokines may trigger recruitment of macrophages and dendritic cells to eliminate infectious agents including apoptotic and pyroptotic cells. Although a part of infected cells could escape from apoptosis possibly by anti-apoptotic viral protein NS1, it is possible that type I IFN inhibits the virus spread through pyroptotic cell death to eliminate infected cells at late phases of infection. Further, the epithelial surfaces of respiratory tissues are exposed to the external environment including commensal microorganisms. It is possible that type I IFN signaling may guarantee the inflammatory response specific for pathogenic infectious agents.

Chapter III. Inflammasome by MxA restricts influenza A virus infection in respiratory epithelial cells

1. Introduction

1-1 Inflammasome receptor in respiratory epithelial cells is unknown

NLRP3 inflammasome, which consists of inflammasome receptor NLRP3, adaptor protein ASC, and caspase-1, is crucial for IAV pathogenesis through proinflammatory cytokine secretion from macrophages (29, 65-67). However, the exact mechanism of inflammasome activation in respiratory epithelial cells, especially a sensor molecule for IAV infection, is largely unknown.

Inflammasome receptors including NLRP3, absent in melanoma 2 (AIM2), and interferon gamma inducible protein 16 (IFI16) have been extensively characterized in monocytes and macrophages against viral infection (29, 68, 69). NLR family CARD domain containing 4 (NLRC4) and NLRP9b are specifically expressed in intestinal epithelial cells and recognizes infectious agents and forms inflammasome complexes (70, 71). Although RIG-I activates inflammasome through a type I IFN-positive feedback loop in respiratory epithelial cells (43), induction of pro-inflammatory cytokines as an inflammasome receptor has not been proved in respiratory epithelium *in vivo* (Fig. 14).

1-2 MxA exhibits the antiviral activity against a variety of viruses by an unknown mechanism

Mx family proteins are the intracellular restriction factor against a variety of viruses including IAV. Mx expression is controlled by type I/III IFNs (72-74). Although *Mx* genes are evolutionarily conserved in almost all vertebrates and responsible for the antiviral response (72, 74), the subcellular localization of Mx protein contributes to its antiviral specificity (75). For instance, nuclear Mx proteins (e.g., mouse Mx1) protect against viruses that replicate in the nucleus (76-78), whereas human MxA protein is cytoplasmic and has a broad antiviral spectrum (79-81).

Human MxA is a dynamine-like large GTPase and consists of N-terminal GTPase domain, central middle domain, and C-terminal GTPase effector domain (75) (Fig. 15). GTPase domain is connected to an elongated stalk that consists of a four-helix bundle comprising the middle domain and GTPase effector domain. The connection between the GTPase domain and the stalk consists of a bundle signaling element (BSE) (82). The BSE is thought to transmit a signal from the GTPase effector domain to the GTPase domain, and transfers structural changes induced by GTP binding and hydrolysis to the stalk (83). MxA assembles into dimer through stalks and the dimers further oligomerize into extended multimers via additional interfaces formed between the stalks and BSEs of neighboring molecules (84-86). Although mutational analysis revealed that the antiviral activity of MxA depends on GTP binding/hydrolysis, an intact BSE, and oligomerization via the stalk (85, 87-89), detail molecular mechanism of MxA antiviral activity is unknown.

2. Materials and methods

2-1 Reagents

Mouse monoclonal antibody against ASC (Millipore), β-Actin (SIGMA), caspase-1 (R&D systems), NLRP3 (AdipoGen), FLAG (SIGMA), and rabbit polyclonal antibodies against ASC (AdipoGen), IgG (Millipore) were purchased. Rabbit monoclonal antibody against β-catenin (Abcam) was purchased. Mouse monoclonal MxA antibody and rabbit polyclonal antibody against NP were prepared as previously described, respectively (46, 90). Plasmids expressing full-length PB1 (pCAGGS-PB1), PB2 (pCAGGS-PB2), PA (pCAGGS-PA), and NP (pCAGGS-NP) were prepared as previously described (91) and transfection was carried out by electroporation (NEON™ Transfection System; Invitrogen) according to the manufacturers' protocol. For the construction of lentiviral plasmid expressing NLRP3, cDNA was amplified from PCA7-NLRP3 (provided by Dr. Takeshi Ichinohe, The University of Tokyo) with NLRP3 primers. LPS (InvivoGen), nigericin (SIGMA), alum (InvivoGen), poly(dA:dT) (InvivoGen), flagellin (AdipoGen), poly (I:C) (InvivoGen) were purchased.

Primer sequences

NLRP3 Forward 5′-GCCGCTAGCGCCGCCACCATGAAGATGGCAAGCACC-3′

NLRP3 Reverse 5′-GCCGGATCCCTACCAAGAAGGCTCAAAGAC-3′

2-2 Cell culture and viruses

PL16T cells were grown in MCDB153HAA with 0.5 ng/ml epidermal growth factor, 5 μg/ml insulin, 72 ng/ml hydrocortisone, 10 μg/ml transferrin, 20 ng/ml sodium selenium, and 2% fetal bovine serum (45). THP-1 cells were grown in Roswell Park Memorial Institute medium (RPMI) 1640 with 10% fetal bovine serum.

NHBE cells were purchased and the cells were grown in B-ALI™ Growth Medium (Lonza). PBMCs were isolated using Histopaque-1077 (Sigma) gradient centrifugation from heparinized blood of healthy volunteers and were grown in RPMI 1640 with 10% fetal bovine serum, 10 ng/ml GM-CSF (Peprotech). HEK 293T cells were grown in Dulbecco's modified essential medium (DMEM) containing 10% fetal bovine serum. Madin-Darby canine kidney (MDCK) cells were grown in minimal essential medium (MEM) (Sigma) containing 10% fetal bovine serum. Influenza virus A/Puerto Rico/8/34 strain and human adenovirus type 5 (HAdV5) were prepared as previously described (46, 92). Sendai virus was a generous gift from Dr. K. Mizumoto (Kitasato University).

2-3 Mice

hMx-Tg, *Nlrp3*$^{-/-}$, *Casp1/11*$^{-/-}$ mice on C57BL/6 background have been reported previously (93-95). *Nlrp3*$^{-/-}$ and *Casp1/11*$^{-/-}$ mice were purchased from The Jackson Laboratory. *Casp1/11*$^{-/-}$ mice were crossed with hMx-Tg mice to generate homozygous knockouts. All *in vivo* experiments were carried out according to the Guideline for Proper Conduct of Animal Experiments, Science Council of Japan. The protocols for experiments with mice were approved by Animal Care and Use Committee, University of Tsukuba.

2-4 Indirect immunofluorescence assays

Cells were fixed with 3% paraformaldehyde (PFA) for 10 min and permeabilized with 0.5% Triton X-100 in PBS containing 0.2% bovine serum albumin (BSA) for 3 min. After incubation in PBS containing 1% skim milk for 1 h, the cells were incubated with primary antibodies for 1 h. After a washing with PBS

containing 0.1% Tween 20 and 0.2% BSA, the cells were incubated with either Alexa Fluor 488- or 568-conjugated secondary antibodies, respectively (Invitrogen) for 30 min. Images were acquired by confocal laser scanning microscopy (LSM700; Carl Zeiss) using × 63 Apochromat objective.

2-5 Quantitative real-time PCR

Total RNA was isolated from PL16T, THP-1, and NHBE cells by the acid guanidinium phenol chloroform method. cDNA was prepared from purified RNA (1 μg) by using ReverTraAce (Toyobo) with oligo $(dT)_{20}$ primer. Real-time PCR was carried out using SYBR Green Realtime PCR Master Mix-Plus (Roche) in the Thermal Cycler Dice Real-Time PCR system (TaKaRa).

Primer sequences

NLRP3 Forward	5′-CCGTCGTCTTTGAGCCTTCT-3′
NLRP3 Reverse	5′-GATGGATCGCAGCTCTCTCC-3′
18S rRNA Forward	5′-AACGGCTACCACATCCAAGG-3′
18S rRNA Reverse	5′-GGGAGTGGGTAATTTGCGC-3′

2-6 Lentivirus production

Lentiviral expression vector with packaging plasmids was co-transfected into HEK 293T cells and collected the resulting supernatant at 72 h post transfection. After 1 h incubation with 5 μg/ml polybrene at 4 °C, the virus was enriched by centrifugation for at least 1 h at 18,600 × g and resuspended in cell medium. Titers were determined by PL16T cells with serial dilutions of concentrated lentivirus. I determined the GFP and RFP expression of the cells by ArrayScan™ high-content systems (Thermo); for a typical preparation, the titer was an approximate multiplicity

of infection (MOI) of 2.5, which showed approximately over than 95% transduction efficiency.

2-7 ASC specks measurement

For the construction of lentiviral plasmid expressing FLAG-GFP-ASC, cDNA was amplified from PCA7-ASC (provided by Dr. Takeshi Ichinohe, The University of Tokyo) with ASC primers. To establish either PL16T or THP-1 cell lines constitutively expressing FLAG-GFP-ASC, the cells were transduced with lentiviral FLAG-GFP-ASC and selected by growth in the presence of 1 μg/ml puromycin (SIGMA) for 2 weeks and then puromycin-resistant cells were isolated. Either FLAG-GFP-ASC PL16T cells (5×10^3 cells) or FLAG-GFP-ASC THP-1 cells (5×10^4 cells) then seeded in 96-well optical bottom plate (Thermo) and GFP-ASC specks were quantified by ArrayScan^{TM} high-content systems.

Primer sequences

ASC Forward 5′-GGCAGATCTATGGGGCGCGCGCGCGAC-3′

ASC Reverse 5′-GCCGAATTCTCAGCTCCGCTCCAGGTCCT-3′

2-8 High-content shRNA screening

The lentivirus-based shRNA library consists of 27,500 shRNA constructs targeting for 5,043 human genes related to signaling transduction (DECIPHER, Cellecta) was fractionated into more than 300 sub-libraries, and the shRNA lentivirus prepared from each sub-library was transduced to PL16T cells expressing FLAG-GFP-ASC at MOI=2.5 (approximately 95% of transduction efficiency). At 36 h post IAV infection, the number of ASC speck-positive cells was quantified by ArrayScan^{TM} high-content systems (n > 5,000 cells). The sub-libraries showing the inhibition of inflammasome activation were pooled and further fractionated into

smaller sub-libraries for next round screening. Empty shRNA plasmid, pRSI12, was used as a negative control.

2-9 Immunoprecipitation

Cells were crosslinked with 0.5% formaldehyde for 10 min at room temperature, and then lysed by sonication in a buffer containing 20 mM Tris-HCl (pH 7.4), 100 mM NaCl, 30 mM KCl, and 0.1% NP-40. After centrifugation at 15,000 rpm for 10 min, FLAG-GFP-ASC was immunoprecipitated with either anti-FLAG M2 agarose beads (SIGMA), non-specific IgG agarose (SIGMA), or anti-ASC antibody with protein A Sepharose. The immunoprecipitated proteins were eluted by 0.1 mM glycine (pH 3.0).

2-10 Mass spectrometry

Eluted proteins were reduced in 4 mM dithiothreitol (DTT) and 4 mM NH_4CO_3 for 60 min at 37°C, then alkylated with 9 mM iodoacetamide for 30 min at 37°C. Following digestion with trypsin for 16 h at 37°C, peptides were concentrated using C18 Tips according to the manufacturer's protocol and then analyzed by LC-MS/MS on a Q Exactive Hybrid Quadrupole-Orbitrap mass spectrometry system (Thermo). Assignment of observed ions was analyzed with Mascot search software.

2-11 Gene silencing mediated by siRNA

The siRNAs against *MxA* and *Nlrp3* genes were purchased from Life Technologies. Cells were transfected with siRNA using Lipofectamine RNAi Max (Life Technologies) according to the manufacturer's protocol.

siRNA sequences

MxA siRNA #1 Forward	5′-UGUGGGCAAUCAGCCUGCUGCCAUU-3′
MxA siRNA #1 Reverse	5′-AAUGUCAGCAGGCUGAUUGCCCACA-3′
NLRP3 siRNA #1 Forward	5′-ACCGCGGUGUACGUCUUCUUCCUUU-3′
NLRP3 siRNA #1 Reverse	5′-AAAGGAAGAAGACGUACACCGCGGU-3′
NLRP3 siRNA #2 Forward	5′-GGAUUGAAGUGAAAGCCAAAGCUAA-3′
NLRP3 siRNA #2 Reverse	5′-UUAGCUUUGGCUUUCACUUCAAUCC-3′
NLRP3 siRNA #3 Forward	5′-UCCACCAGAAUGGACCACAUGGUUU-3′
NLRP3 siRNA #3 Reverse	5′-AAACCAUGUGGUCCAUUCUGGUGGA-3′

2-12 ASC oligomerization assay

Cells were lysed in PBS buffer containing 0.5% Triton X-100 and the cell lysates were centrifuged at 7,000 × g for 15 min at 4 °C. Supernatants were transferred to new tubes (Triton-X-soluble fractions). The Triton-X-100-insoluble pellets were washed with PBS twice and then suspended in 200 μl PBS. The pellets were then cross-linked at room temperature for 30 min by adding 2 mM bis(sulfosuccinimidyl) suberate (BS_3) (Thermo). These cross-linked pellets were spun down at 7,000 × g for 15 min and dissolved directly in SDS sample buffer and subjected to 12.5% SDS-PAGE for western blotting analysis.

2-13 SparQ cumate switch system

SparQ dual promoter lentivector and CymR repressor lentivector were purchased from System Bioscience (SBI). To construct the plasmid expressing siRNA-resistant MxA, cDNA was amplified using plasmids expressing pCHA-MxA (96) as templates and N-terminal and C-terminal region of MxA primers sets. To construct plasmids expressing siRNA-resistant MxA with mutation of T103A, K554E to K557E (L4), M527D, and L617D, cDNA was amplified using above resultant SparQ pCDH-MxA with T103A, L4, M527D, or L617D primer sets respectively. For

the construction of plasmid expressing mouse Mx1, *Mx1* fragment from pCHA-Mx1 (90) was digested with Eco RI (TOYOBO) and cloned into SparQ pCDH. To establish PL16T cell line constitutively expressing CymR repressor and inducible SparQ expression with the appropriate gene (identified above), the cells transduced with lentiviral CymR repressor and selected by puromycin for 2 weeks. Puromycin-resistant cells again transduced with lentiviral SparQ expression with appropriate gene and selected by the puromycin for 2 weeks. At 6 h post IAV infection, 30 μg/ml 4-isopropylbenzoic acid (cumate) (SIGMA) was added to stimulate target gene expression.

Primer for siRNA-resistant MxA

N-terminal region of MxA Forward	5′-CCGGAATTCGCCGCCACCATGGTTGTTTCCGAAGTGG-3′
N-terminal region of MxA Reverse	5′-GATATCGGCTGGTTGGTTACCAACAGCCACTCTGGTTAT-3′
C-terminal region of MxA Forward	5′-GTTGGTAACCAACCAGCCGATATCGGGTATAAGATCAAG-3′
C-terminal region of MxA Reverse	5′-CGAGGATCCTTAACCGGGGAACTGGGC-3′

Primer for MxA mutagenesis

T103A Forward	5′-CCCAGAGGCAGCGGGATCGTGGCCAGATGCCCGCTGGTG-3′
T103A Reverse	5′-TTTCAGCACCAGCGGGCATCTGGCCACGATCCCGCTGCC-3′
L4 Forward	5′-GAGAAGGAGCTGGAAGAAGAAGAGGAGGAGGAGTCCTGGGATTTTGGG-3′
L4 Reverse	5′-GAAAGCCCCAAAATCCCAGGACTCCTCCTCCTCTTCTTCTTCCAGCTC-3′
M527D Forward	5′-CTGATCCGCCTCCACTTCCAGGATGAACAGATTGTCTAC-3′
M527D Reverse	5′-CTGGCAGTAGACAATCTGTTCATCCTGGAAGTGGAGGCG-3′
L617D Forward	5′-CAGCAGCTTCAGAAGGCCATGGATCAGCTCCTGCAGGAC-3′
L617D Reverse	5′-GTCCTTGTCCTGCAGGAGCTGATCCATGGCCTTCTGAAG-3′

2-14 Cytokine measurements

Cytokines were measured by ELISA with either human IL-1β (R&D system), human IL-18 (MBL), or mouse IL-1β (R&D system) according to the manufacturers' instruction.

2-15 Infection of mice

Eight-week-old mice were anesthetized by intraperitoneal injection of pentobarbital sodium and then infected with IAV in 50 μl of PBS via intranasal administration.

2-16 Bone marrow transplantation

Recipient mice were irradiated with 2 doses of 4.5Gy using MBR-1520R irradiator (Hitachi). The next day, bone marrow was collected from donor mice. Collected bone marrow cells were then washed with sterile PBS containing 1% fetal bovine serum (FBS) and 5×10^5 bone marrow cells in sterile PBS were injected into the tail vein of irradiated recipient mice. At 8 weeks post bone marrow transplantation, the chimeric mice were infected with IAV.

2-17 Flow cytometry analysis

Cells were collected from bronchoalveolar lavage (BAL) and resuspended in red blood cells (RBC) lysis buffer (154 mM NH_4Cl, 10 mM $KHCO_3$, and 0.1 mM EDTA) for 5 min. After washing the cells with PBS containing 2% FBS, the cells were stained with either anti CD45.2 (Biolegend), anti Mac-1 (CD11b) (Biolegend), or anti IgG2a (Biolegend) antibodies for 30 min on ice. To confirm the transplanted engraftment, the cells were collected from bone marrow of chimeric mice. After washing the cells with PBS containing 2% FBS, the cells were fixed, permeabilized, and incubated with APC-conjugated anti-mac-1 and anti-NLRP3 antibodies for 1 h. After a washing, the cells were incubated with Alexa Fluor 488-conjugated secondary

antibody (Invitrogen) for 30 min. Flow cytometric analysis was performed using a Guava easyCyto flow cytometer (Merck Millipore).

2-18 Plaque assay

A confluent monolayer culture of MDCK cells in a 6-well tissue culture plates was washed with serum-free MEM and then was infected with IAV. After virus adsorption at 37°C for 1 h, the cells were washed with serum-free MEM and then added with MEM containing 0.8% agarose, 0.2% BSA, 1 × vitamin (Gibco), and 1 μg/ml TPCK-treated trypsin (Sigma). After incubation at 37°C for 3 days, cells were fixed with ethanol-acetic acid (1:1) solution and stained with 0.5% amide black 10B.

2-19 Histology and immunohistochemical staining

Mice were infected with 3,000 PFU of IAV. Four-μm paraffin lung tissue sections were stained with hematoxylin and eosin. The samples were observed using BZ-X700 microscopy (KEYENCE). For immunohistochemical staining, the sections were deparaffinized, and then antigen retrieval was performed in a citrate buffer (0.1 M citric acid and 0.1 M sodium citrate) at 121°C for 3 min. After incubation in PBS containing 1% skim milk for 1 h, the tissue sections were incubated with mouse anti-ASC and rabbit anti-β-catenin antibodies for 1 h. After a washing with PBS containing 0.1% Tween 20 and 0.2% BSA, the tissue sections were incubated with Alexa Fluor 488-conjugated anti-rabbit IgG and Alexa Fluor 568-conjugated anti-mouse IgG antibodies for 30 min. Images were acquired by confocal laser scanning microscopy (LSM700; Carl Zeiss) using × 63 Apochromat objective.

2-20 Statistical analysis

Statistical significance was tested using a two-tailed Student's t-test. n/s, not significant. ***P < 0.001, **P < 0.01. Survival curves were analyzed using a log-rank (Mantel–Cox) test. For the pairwise comparison with multiple testing, I analyzed with two-way ANOVA statistical methods.

3. Results

3-1 NLRP3 does not promote inflammasome assembly in respiratory epithelial cells against IAV infection

NLRP3 is a major inflammasome receptor against IAV infection in dendritic cells and macrophages (29, 65-67). Influenza viral protein M2 channel activity causes the activation of the NLRP3 inflammasome by IAV and is sufficient to stimulate inflammasome in macrophages and dendritic cells (97). To evaluate the requirement for the NLRP3 in inflammasome in respiratory epithelial cells, I examined the amount of human *Nlrp3* mRNA in THP-1, PL16T, and NHBE cells induced by IAV infection. The *Nlrp3* mRNA was expressed in THP-1 cells, but it was not expressed both in PL16T and NHBE cells (Fig. 16A). Further, ASC specks, a micrometer-sized ASC assembly, were induced by NLPR3 in THP-1 cells, but not in PL16T cells (Fig. 16B and C), suggesting that NLRP3 does not function as an inflammasome receptor in respiratory epithelial cells against IAV infection.

3-2 Identification of MxA as a novel inflammasome receptor in respiratory epithelial cells upon IAV infection

To identify a novel respiratory epithelium-specific inflammasome receptor, I performed a high-content shRNA library screening and a proteomic analysis of ASC-interacting proteins upon IAV infection. I firstly performed high-content genome-wide shRNA screening (Fig. 17A) using constitutively expressing FLAG-GFP-ASC PL16T that showed similar cell death phenotype with NHBE in viral infection (Fig. 5 and 7). The library consists of 27,500 shRNA expression constructs, targeting 5043 genes (five to six shRNA sequences per gene). Using *Escherichia coli* (*E. coil*)

colony fractionation and plasmid miniprep, the library was fractionated into more than 300 sub-libraries, and the shRNA lentivirus prepared from each sub-library was transduced to PL16T cells expressing FLAG-GFP-ASC at MOI=2.5 (approximately 95% of transduction efficiency) (Fig. 17B). At 36 h post IAV infection, ASC speck was quantified by high-content microscopy. The sub-libraries showing the inhibition of inflammasome activation were pooled and further fractionated into smaller sub-libraries for next round screening. I finally identified 5 target genes including *CTSL1*, *MOGS*, *PTPN7*, *Sertad2*, and *MxA* that were markedly reduced GFP-ASC specks in PL16T cells against viral infection by these knockdown genes (Fig. 17C and D). By contrast, 5 target genes had no effect on GFP-ASC specks reduction in infected THP-1 cells (Fig. 17E).

The liquid chromatography–mass spectrometry (LC-MS) analysis was used to observe the interacting proteins of ASC, universal inflammasome component. When ASC specks were observed in approximately 45% upon IAV infection (Fig. 18A), FLAG-GFP-ASC from PL16T and THP-1 cells was immunoprecipitated with anti-FLAG agarose beads. Immunoprecipitated proteins were subjected to SDS-PAGE for silver staining (Fig. 18B) and LC-MS (Fig. 18C). I identified 113 proteins including MxA that were specifically binds to ASC in infected PL16T cells (Fig. 18C). MxA was alone identified that was sufficient to promote the inflammasome formation and interacted with ASC in infected respiratory epithelial cells. The interaction between MxA and endogenous ASC was confirmed by immunoprecipitation using anti-ASC antibody (Fig. 19A). Further, MxA co-localized with ASC specks in infected PL16T cells at 36 h post infection (Fig. 19B).

3-3 MxA is sufficient to stimulate inflammasome in respiratory epithelial cells

MxA is a type I/III interferon-inducible protein and exhibits the antiviral activity against a variety of viruses including IAV by an unknown mechanism (79-81, 98, 99). To elucidate whether MxA is required for the inflammasome activation in respiratory epithelial cells, I examined downstream signals of inflammasome activation, cleaved form of caspase-1 and the secretion of IL-1β and IL-18. Consistent with previous reports (65, 67), I found that secretion of IL-1β in primary human peripheral blood mononuclear cells (PBMC)-derived macrophages and IL-18 in THP-1 cells induced by IAV infection was induced by NLRP3 (Fig. 20A and B). By contrast, secretion of IL-1β in NHBE cells and IL-18 in PL16T cells induced by IAV infection was regulated by MxA (Fig. 20C and D). Although caspase-1 was cleaved in both IAV infected-respiratory epithelial cells and macrophages, MxA did not regulate cleaved forms of caspase-1 in macrophages due to its no expression (Fig. 20E). I further tested whether MxA knockdown is rescued by exogenous expression of NLRP3 in PL16T cells. Using lentiviral overexpression of NLRP3, which can promote NLRP3 inflammasome in NLRP3 deficient cells (48), I found that the reduction of IL-1β secretion by MxA knockdown was complemented by NLRP3 expression (Fig. 21 lanes 7 and 8). Taken together, these finding strongly suggest that MxA is required for the inflammasome in respiratory epithelial cells against IAV infection.

3-4 MxA recognizes NP as a viral ligand to assembly inflammasome

To elucidate mechanism by which ligands can activate the MxA inflammasome, I examined IL-1β secretion in lipopolysaccharide (LPS)-primed THP-1 and PL16T cells in the presence of various stimuli to other inflammasome receptors; nigericin and alum for NLRP3 inflammasome, poly(dA:dT) for AIM2 inflammasome,

and flagellin for NLRC4 inflammasome. As previously reported (100, 101), IL-1β secretion induced by IAV infection, nigericin, or alum were abolished in NLRP3 knockdown THP-1 cells, but IL-1β release in response to poly(dA:dT) and flagellin was not affected in NLRP3 knockdown THP-1 cells (Fig. 22A). In contrast, the IL-1β secretion was not observed upon various stimuli to other inflammasome receptors in PL16T cells (Fig. 22B). In addition, IL-1β secretion was triggered by infection with adenovirus (ADV; DNA virus) and sendai virus (SeV; RNA virus) in an MxA-dependent manner in PL16T cells (Fig. 23).

It is previously reported that MxA interacts with viral ribonucleoprotein complexes consisting of viral polymerases and nucleoprotein (NP) (90). To determine a viral ligand recognized by MxA inflammasome, I next transfected NP and viral polymerase subunits including PA, PB1, and PB2 with poly I:C, a potent type I IFN inducer. ASC specks were observed in cells transfected with NP, but not viral polymerases (Fig. 24). These findings strongly suggest that MxA functions as a viral infection-specific pathogen sensor protein in respiratory epithelial cells and MxA recognizes NP as a viral ligand to assembly inflammasome against IAV infection.

3-5 Oligomerization of MxA is required for the inflammasome formation

Upon inflammasome activation, ASC assembles into Triton X-100-insoluble homo-oligomer, and the oligomerized ASC is required for caspase-1 activation. To analyze the extent of ASC oligomerization, 0.5% Triton X-100-treated PL16T cells were crosslinked with 2 mM bis(sulfosuccinimidyl) suberate and analyzed by western blotting with anti-ASC antibody. Most ASC in the Triton-insoluble fraction was highly oligomerized in infected control cells, but not in infected MxA knockdown

cells (Fig. 25A). Corresponding to this, the proteolytic activation of caspase-1 was not found in infected MxA knockdown cells (Fig. 25B).

MxA is a dynamine-like large GTPase and consists of N-terminal GTPase domain, central middle domain, and C-terminal GTPase effector domain (75) (Fig. 15). MxA assembles into homo-oligomers through the interaction between central middle domain and C-terminal GTPase effector domain (86). The L4 loop (533-561 a.a. position) of MxA is required to associate with ER-Golgi intermediate compartments (87). To address the molecular mechanism, ASC oligomerization (Fig. 27A), ASC speck formation (Fig. 27B), and IL-1β secretion (Fig. 27C) were examined with MxA knockdown PL16T cells expressing siRNA-resistant MxA mutants using lentiviral SparQ cumate switch system as following: GTP binding-deficient mutant (T103A) (89); membrane binding-deficient mutant (K554E, K555E, K556E, and K557E in L4 loop (L4)) (102); monomeric mutant (M527D) (85); dimeric mutant (L617D) (85). Expression of siRNA-resistant wild-type (WT) MxA allowed to rescue the reduction of MxA expression (Fig. 26, lane 8) and inflammasome formation in infected MxA knockdown cells (Fig. 27A, lane 4; Fig. 27B, lane 4; Fig. 27C, lane 4). In contrast, the ASC speck formation partially increased to 20-40% of that of WT expression by the expression of GTP binding-deficient mutant and membrane binding-deficient mutant (Fig. 27B, lanes 5 and 6), suggesting that the GTPase activity and the membrane binding activity are important to fully activate the inflammasome formation. Of interest, the expression of monomeric and dimeric MxA mutants resulted in the monomeric and dimeric ASC in the Triton-insoluble fraction, respectively (Fig. 27A, lanes 7 and 8). This strongly suggests that ASC assembles into the homo-oligomers dependent on the extent of MxA oligomerization. Note that the expression of mouse Mx1 did not complement

the reduced ASC specks and IL-1β secretion in infected MxA knockdown cells (Fig. 28A and B), suggesting that MxA inflammasome may be conserved among a part of vertebrates expressing cytoplasmic Mx1/MxA protein.

3-6 Leukocytes in hMx-Tg mice migrate into the bronchioles to remove IAV at the early phages of viral infection

Most inbred mouse strains carry an inactive *Mx1* gene due to a large deletion of exons or a nonsense mutation (103). I next examined *in vivo* function of MxA inflammasome with a transgenic mouse carrying the entire human *Mx* locus except *MxB* gene (hMx-Tg) (93). In this mouse line, MxA is induced by endogenous type I/III IFNs. As reported previously (93), hMx-Tg mice were highly resistant to IAV infection compared with non-transgenic (non-Tg) mice (Fig. 29A and B). Macroscopically, the degree of hemorrhage and congestion in the lungs of hMx-Tg mice was much weaker than those in non-Tg mice at day 5 and day 7 post-infection (Fig. 30). The histological analysis of lung slices revealed that non-Tg mice did not show obvious pathogenic changes at 3 days post infection, but did show severe bronchiolitis reducing the alveolar air space, leukocyte infiltration, and desquamation of the bronchiolar epithelium at day 5 post-infection (Fig. 31, upper panels). In contrast, in hMx-Tg mice, a massive infiltration with neutrophils and mononuclear inflammatory cells was observed in the bronchiolar regions at day 3 post-infection (Fig. 31, lower panels), and the extent of bronchiolitis was dramatically reduced compared with non-Tg mice at day 5 post-infection. To quantify the extent of leukocyte infiltration, we further examined the number of leukocytes into bronchoalveolar lavage (BAL) by FACS analysis using anti-CD45.2 antibody as a leukocyte marker. As expected, the number of infiltrating leukocytes obtained from

hMx-Tg mice was peaked at 3 days post infection, but that of non-Tg mice was at 7 days post infection (Fig. 32). These results suggest that human MxA in bronchiolar epithelial cells may functions to recruit leukocyte and represses virus spread from the bronchioles to distal alveolar regions.

3-7 Human MxA is an inflammasome sensor *in vivo* against IAV infection

To assess whether antiviral activity of MxA in hMx-tg mice is dependent on the inflammasome, I generated hMx-Tg × *Casp1/11*$^{-/-}$ mice. Compared with non-Tg mice, Mx-Tg mice exhibited about 3 times high level of IL-1β secretion and total BAL leukocytes. Interestingly, IL-1β secretion and leukocytes recruitment induced by IAV infection were diminished similarly in *Casp1*$^{-/-}$ or hMx-Tg × *Casp1*$^{-/-}$ mice (Fig. 33A and B). In contrast, pulmonary viral titer in hMx-Tg mice was highly decreased than that of non-tg mice, and the viral titer was increased similarly in *Casp1*$^{-/-}$ or hMx-Tg × *Casp1*$^{-/-}$ mice (Fig. 33C). Importantly, hMx-Tg mice were survived against IAV infection, whereas *Casp1/11*$^{-/-}$ and hMx-Tg × *Casp1/11*$^{-/-}$ mice lost weight and died day 8 or day 10, respectively (Fig. 33D and E), suggesting that human MxA reveals inflammasome sensor *in vivo* against IAV infection.

3-8 MxA is required for the inflammasome activation in respiratory epithelial cells *in vivo*

To investigate the relative contributions of the MxA inflammasome in respiratory epithelium against IAV infection, I carried out bone marrow transplantation from *Nlrp3*$^{-/-}$ mice to hMx-Tg recipient mice to exclude the inflammasome response in immune cells. The chimeric mice showed approximately 90% of engraftment of bone marrow (Fig. 34A and B), and the level of IL-1β

secretion and total BAL leukocytes was comparable between chimeric and non-chimeric mice (Fig. 34C and D).

The infected non-Tg recipient mice transplanted with *Nlrp3*$^{-/-}$ bone marrow cells did not induce IL-1β secretion and leukocytes recruitment in BAL, suggesting that IL-1β secretion and leukocytes recruitment were only stimulated from immune cells in an NLRP3-dependent manner. In contrast, the IL-1β secretion and leukocytes recruitment were still observed in hMx-Tg mice transplanted with *Nlrp3*$^{-/-}$ bone marrow cells (Fig. 35A and B). Further, ASC specks were observed in bronchiolar epithelial cells in hMx-Tg mice but not in non-Tg mice at 3 days post infection (Fig. 35C, arrowheads). These findings indicate that MxA is required for the inflammasome activation in the respiratory epithelium upon IAV infection *in vivo*.

4. Discussion

Using IAV infection as a model, I used high-content genome-wide shRNA screening and proteomic analysis to identify the genes for inflammasome receptor and identified MxA in respiratory epithelial cells. Although NLRP3 is a major inflammasome sensor in macrophages (Fig. 20) (29, 65-67), MxA in respiratory epithelial cells selectively forms inflammasome complexes with the ASC and caspase-1 to promote pro-inflammatory responses against IAV infection (Fig. 19, 20, 25, and 36).

ASC and NLRP3 are the members of the pyrin domain (PYD) subfamily that ASC contains a PYD and a caspase recruitment domain (CARD), and NLRP3 has a PYD, a nucleotide-binding oligomerization domain, and a leucine-rich repeat domain (Fig. 14). Upon recognition of danger signals, ASC and NLRP3 interact through their PYD domains, and ASC and caspase-1 binding is mediated by a CARD-CARD interaction. ASC then assembles into the homo-oligomers to form inflammasome. (104) (Fig. 14). MxA carries GTPase domain, MD, and GED, which include neither PYD nor CARD (75) (Fig. 15). Although either expression of monomeric or dimeric MxA mutants resulted in monomeric or dimeric ASC, respectively (Fig. 27A), and MxA-ASC interaction and co-localization were found in infected PL16T cells (Fig. 19), direct MxA-ASC interaction was not observed. It is still open questions of how MxA binds with ASC to form the inflammasome upon the viral infection.

My studies also highlight that human MxA reveal the inflammasome sensor in respiratory epithelium *in vivo* against IAV infection. Human MxA inflammasome in bronchiolar epithelial cells stimulates IL-1β secretion that functions to recruit leukocyte in bronchioles to eliminate IAV at the early phases of viral infection. A

failure to induce MxA inflammasome in respiratory epithelial cells likely explains how this innate host response is undermined and contributes to IAV pathogenesis.

Chapter IV. Conclusion and perspectives

1. Conclusion

The respiratory epithelium is exposed to the external environment and functions as a sensor of infectious agents to initiate inflammatory response. IAV is an important human respiratory pathogen that infects millions of people worldwide in seasonal epidemics. NLRP3 inflammasome, which consists of inflammasome receptor NLRP3, adaptor protein ASC, and caspase-1, is crucial for IAV pathogenesis through proinflammatory cytokine secretion from macrophages. However, the exact mechanism of inflammasome activation in respiratory epithelial cells, especially a sensor molecule for IAV infection, is largely unknown.

My studies revealed that MxA functions as a novel inflammasome receptor in respiratory epithelial cells upon IAV infection. MxA recognizes NP viral protein as a pathogen-associated ligand, and oligomerization of MxA is required for the inflammasome formation in respiratory epithelial cells but not macrophages. The expression of human MxA *in vivo* activated the inflammasome formation in bronchiolar epithelial cells and protected mice from IAV infection by repressing virus spread from the bronchioles to distal alveolar regions. My study highlights the significance of epithelial inflammatory response mediated by MxA inflammasome, and human Mx-transgenic mice can be a valuable animal model for human respiratory epithelium to demonstrate inflammatory response upon virus infection.

2. Perspectives

The past decade has brought a great expansion in our understanding of innate sensing and responses to IAV infection. In particular, several studies reveal the importance of inflammasome in innate defenses against viral infection (65-67). Furthermore, we now begin to learn about the underlying mechanisms of MxA dependent inflammasome activation in respiratory epithelial cells against IAV infection. Although some progress has been made in this regard, additional studies of MxA inflammasome are required and many questions remain to be answered. How and why the MxA inflammasome is required to mediate protection against IAV infection? Is there crosstalk with other PRRs? What are other viral triggers responsible for MxA inflammasome activation? Addressing these and other questions regarding IAV recognition through MxA and potentially other inflammasome complexes should provide evidences to making more effective vaccines and therapeutics against impending IAV pandemics.

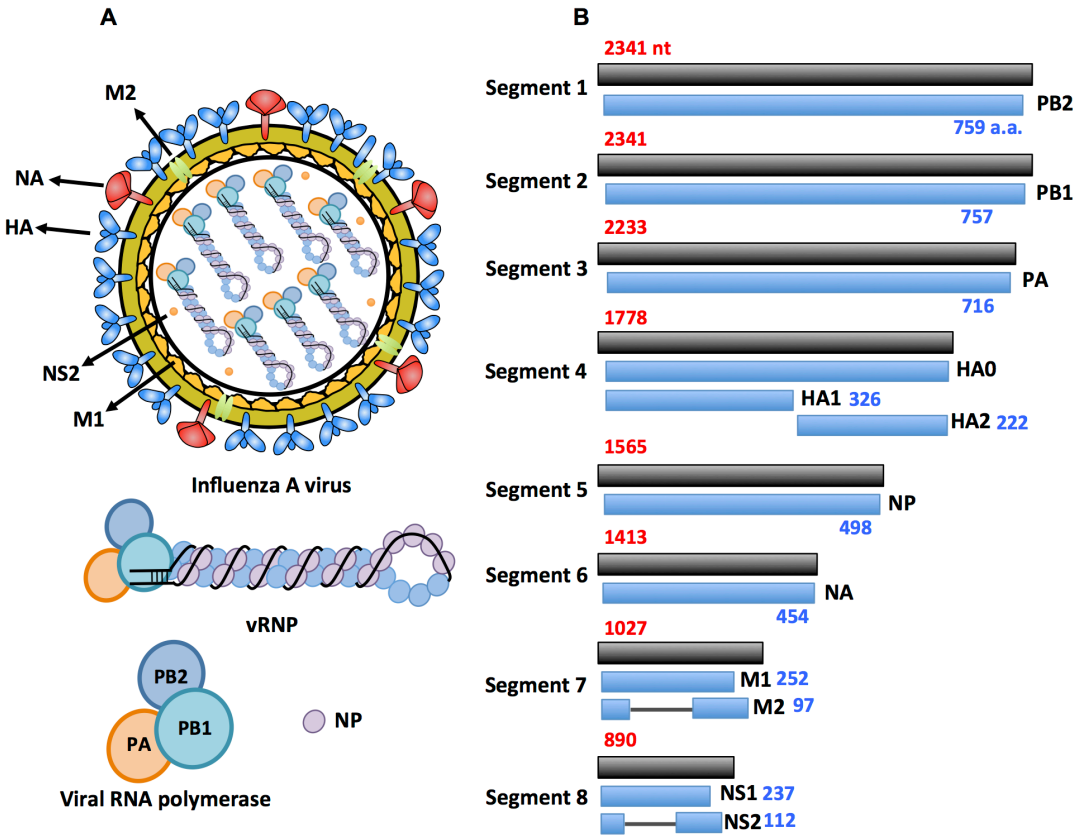

Figure 1 Structure of influenza A virus

(A) Structure of influenza A virus (IAV). IAV contains eight-segmented and single- and negative-stranded RNAs (vRNA) as its genome. Each segment is encapsidated by NP and associated with the RNA polymerase to form viral ribonucleoprotein (vRNP) complex. The vRNP complex (PB1, PB2, PA, and NP) is a basic unit for both transcription and replication. (B) Structure of viral genome.

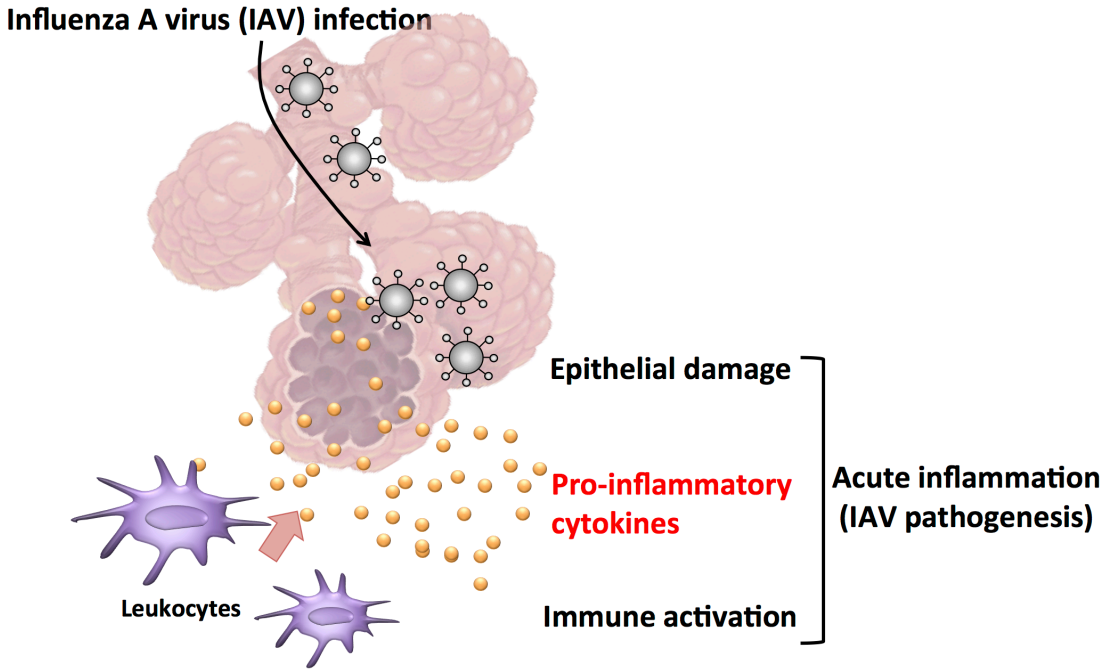

Figure 2 Influenza A virus pathogenesis.

IAV induces inflammatory responses as a result of respiratory epithelial cell death. The pro-inflammatory cytokines from respiratory epithelial cells trigger recruitment of leukocytes including macrophages and neutrophils to remove infectious agents. These migrated leukocytes contribute to excessive inflammation, which leads to pneumonia.

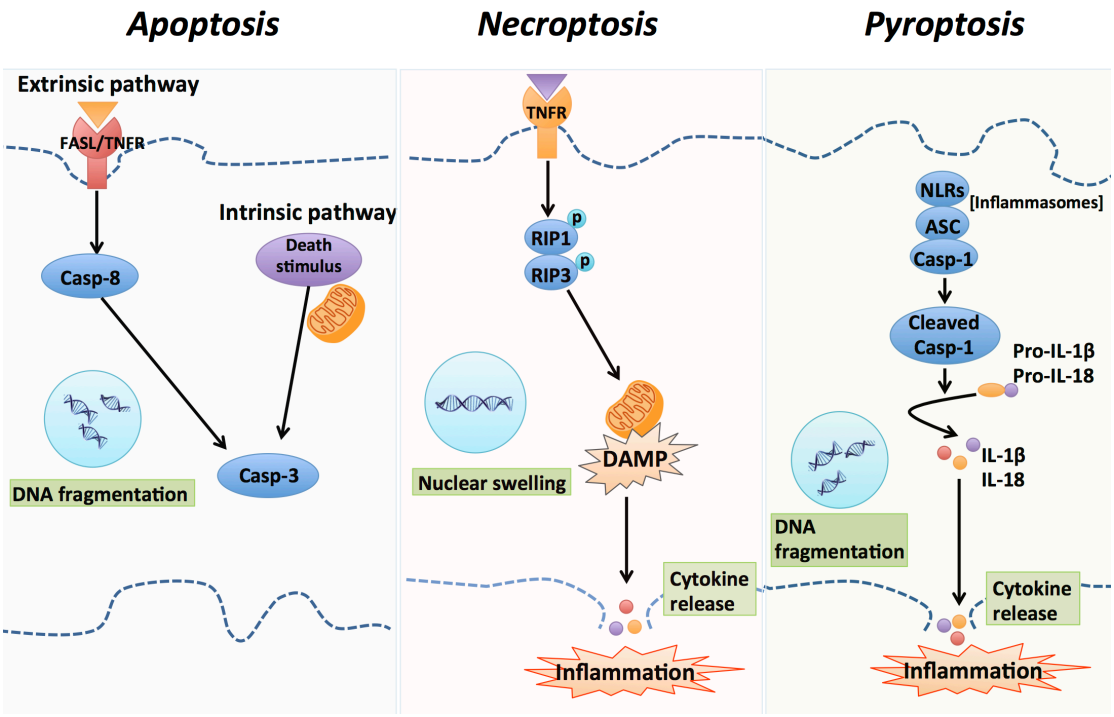

Figure 3 Overviews of programmed cell death pathways.

Apoptosis, immunologically silent cell death, is triggered by the extrinsic pathway and the intrinsic pathway that selectively cleave caspase-3 to produce morphological features associated with apoptosis such as DNA fragmentation. Necroptosis, caspase-independent inflammatory cell death, is controlled by RIP1 and RIP3 kinases complex that stimulates DAMPs as a danger signal to neighbor cells. Pyroptosis is a caspase-1-dependent inflammatory cell death controlled by inflammasomes, multiprotein complexes consisting of caspase-1, ASC, and PRRs such as NOD-like receptors (NLRs) family proteins. Inflammasome induces proteolytic cleavage of pro-caspase-1 that cleaves its substrates, IL-1β and IL-18 for the inflammation.

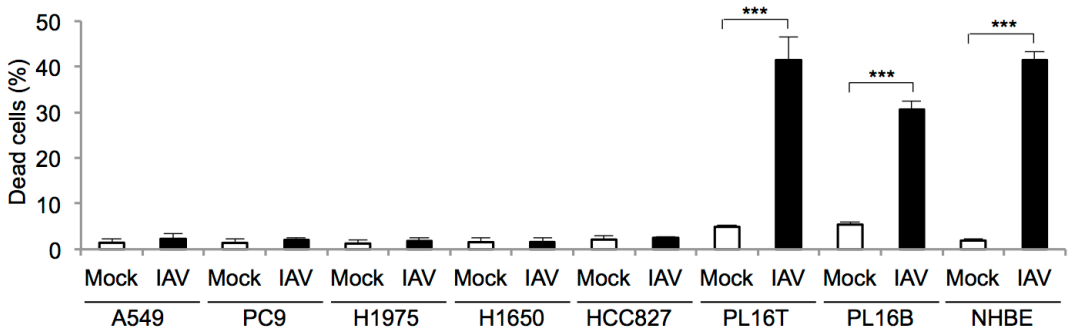

Figure 4 Cell death in malignant tumor cell lines was rarely induced by IAV infection.

Number of dead cells by IAV infection in human malignant respiratory epithelial cells (A549, PC9, H1975, H1650, HCC827), human atypical adenomatous hyperplasia (AAH) respiratory epithelial cells (PL16T), human non-neoplastic respiratory epithelial cells (PL16B), and primary normal human bronchial epithelial cells (NHBE) were determined by trypan blue dye exclusion assays. The data represent averages with standard deviations from three independent experiments ($n > 100$). ***$P < 0.001$ by Student's t test.

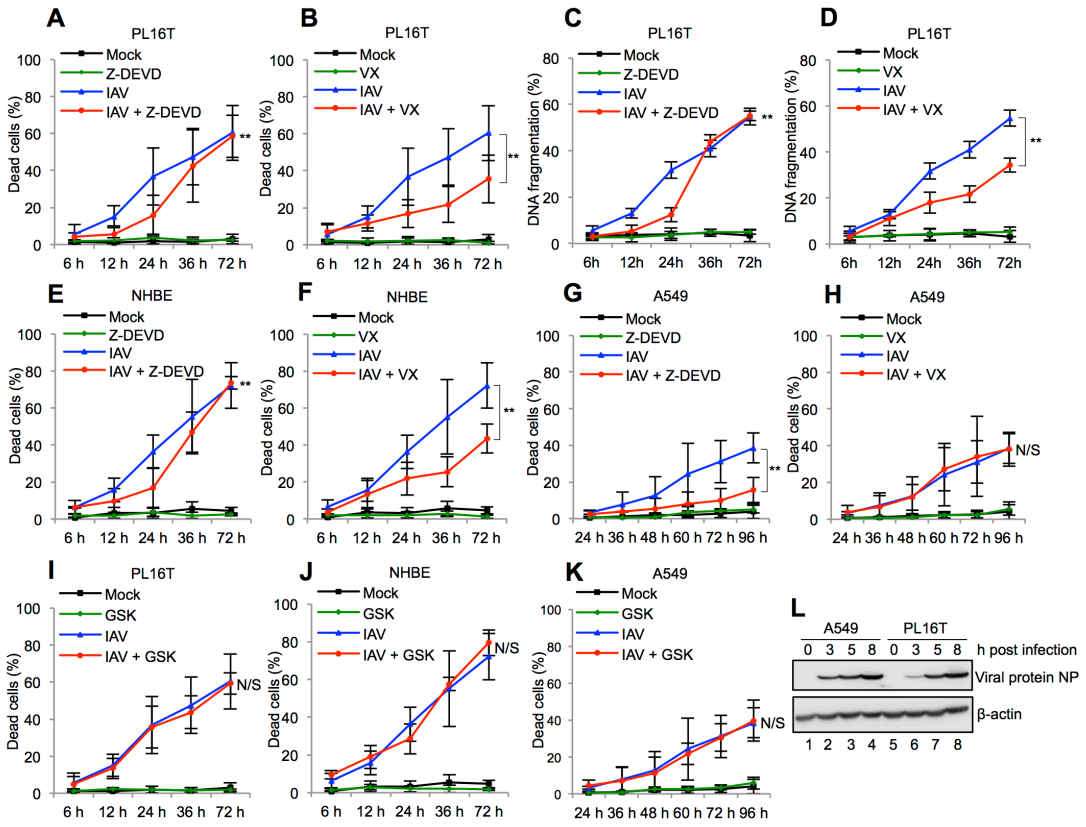

Figure 5 IAV infection induces pyroptotic cell death in precancerous respiratory epithelial cells.

(A to K) PL16T cells (A, B, C, D, and I), NHBE cells (E, F, and J), and A549 cells (G, H, and K) were infected with IAV at MOI of 10 in the presence of 10 μM Z-DEVD-FMK (A, C, E, and G; Z-DEVD), 20 μM VX-765 (B, D, F, and H; VX), and 3 μM GSK-872 (I, J, and K; GSK). The number of dead cells was measured by trypan blue dye exclusion assays and the number of DNA fragmented cells stained with Hoechst 33342 was quantified by ArrayScan^{TM} high-content systems. The data represent averages with standard deviations from three independent experiments ($n > 100$). **$P < 0.01$ by two-way ANOVA. n/s, not significant. (L) At 3, 5, 8 h post infection, infected A549 (lanes 1-4) and PL16T cells (lanes 5-8) were lysed, and the lysates were analyzed by SDS-PAGE followed by western blotting assays using anti-NP and anti-β-actin antibodies.

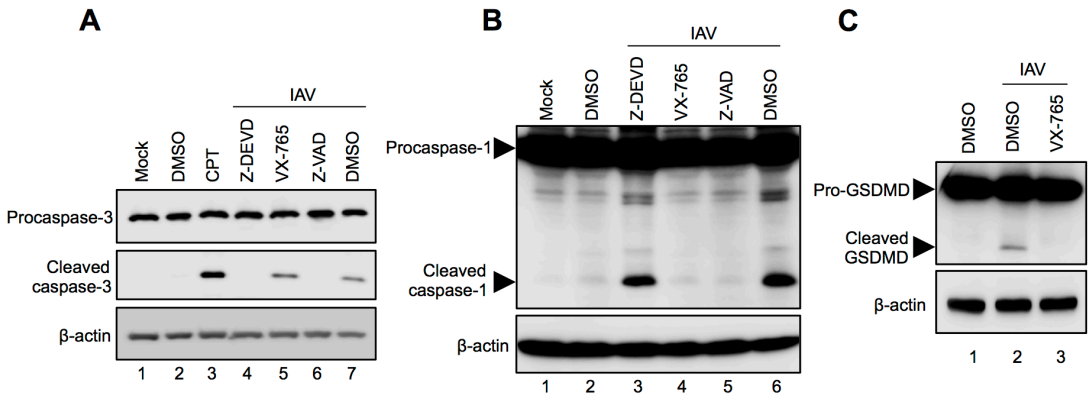

Figure 6 Apoptosis and pyroptosis are induced in PL16T cells by IAV infection

(A) Infected PL16T cells were incubated with either 10 μM Z-DEVD-FMK, 20 μM VX-765, or 20 μM Z-VAD-FMK for 24 h and then the cell lysates were subjected to western blot analysis with anti-procaspase-3 and anti-cleaved caspase-3 antibodies. As a positive control, cells were treated with 10 μM camptothecin (CPT) to activate caspase-3. β-actin was detected as a loading control. (B) Infected PL16T cells were incubated with either 10 μM Z-DEVD-FMK, 20 μM VX-765, or 20 μM Z-VAD-FMK for 48 h and then the cell lysates were subjected to western blot analysis using anti-caspase-1 antibody. β-actin was detected as a loading control. (C) Infected PL16T cells were incubated with 20 μM VX-765 for 48 h and then cell lysates were subjected to western blot analysis using GSDMD antibody. β-actin was detected as a loading control.

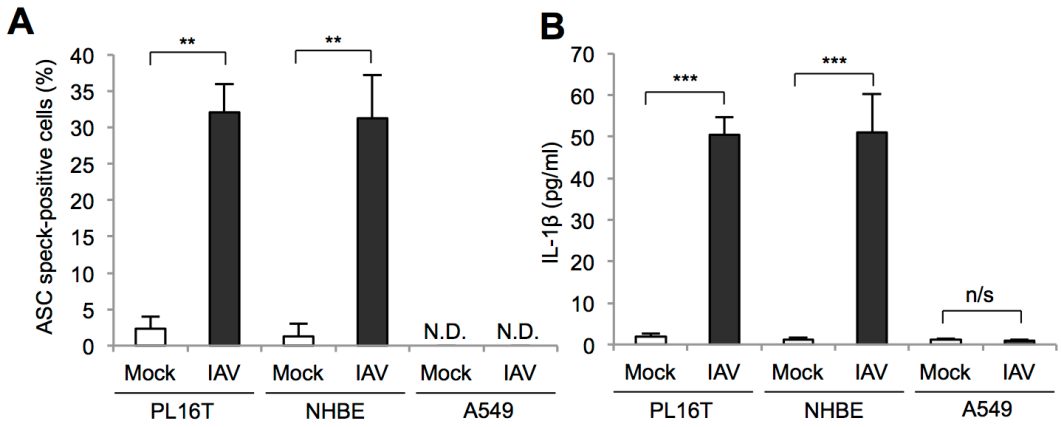

Figure 7 IAV infection induces inflammasome assembly and IL-1β secretion in human respiratory epithelial cells.

(A) At 48 h post infection, uninfected and infected PL16T, NHBE, and A549 cells were subjected to indirect immunofluorescence assays using anti-ASC antibody and percent of ASC speck-positive cells were quantified. The data represent averages with standard deviations from three independent experiments (n > 100). (B) PL16T, NHBE, and A549 cells were infected with IAV at MOI of 10. At 72 h post infection, cell-free supernatants were collected and the concentration of IL-1β was quantified by ELISA. The data represent averages with standard deviations from three independent experiments. **P < 0.01, ***P < 0.001 by Student's t test. N.D., not detected. n/s, not significant.

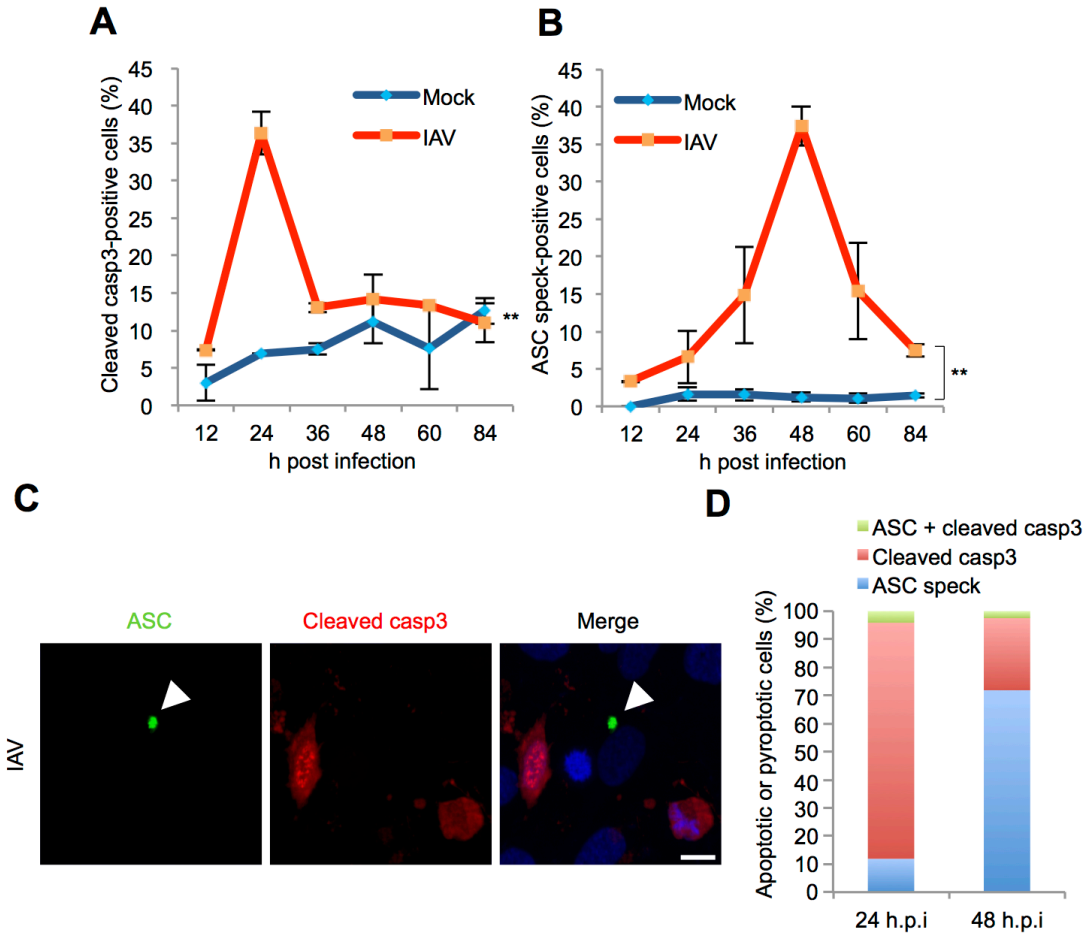

Figure 8 Apoptosis and pyroptosis are independently induced in PL16T cells against IAV infection.

(A to D) At 12, 24, 36, 48, 60, and 84 h post infection, uninfected and infected PL16T cells were subjected to indirect immunofluorescence assays with anti-ASC (green) and anti-cleaved caspase-3 (red) antibodies. The average number of cleaved caspase-3-positive (A) and ASC speck-positive (B) cells and standard deviations obtained from three independent experiments are shown (n > 100). The representative result at 24 h post infection is shown in (C). Arrowheads indicate ASC inflammasome. Scale bar, 10 μm. The percentage of cleaved caspase-3-positive (red), ASC speck-positive (blue), and cleaved caspase-3/ASC speck-positive cells (green) are counted at 24 and 48 h post infection (D). **P < 0.01 by two-way ANOVA.

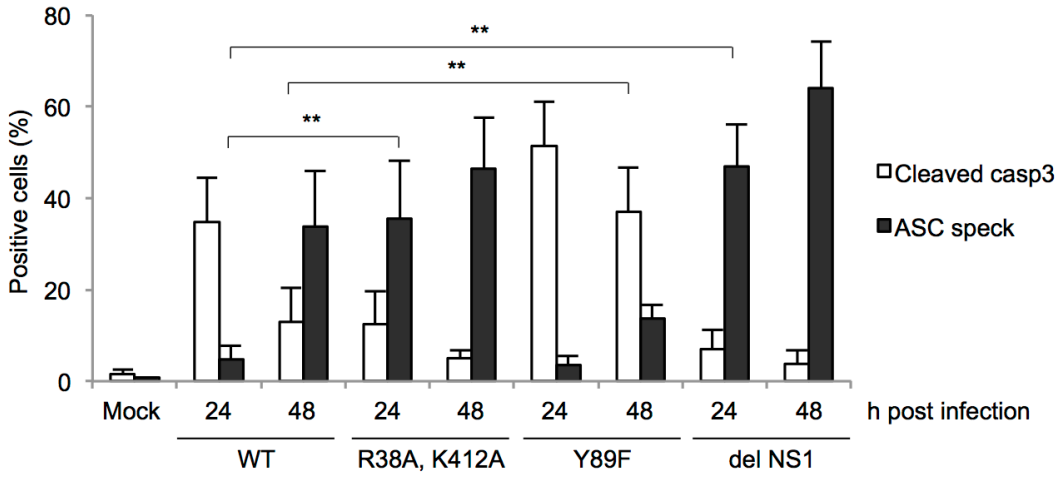

Figure 9 Apoptotic and pyroptotic cell death of respiratory epithelial cells induced by NS1 mutant viruses.

PL16T cells were infected with either wild-type (WT), R38A/K41A, Y89F, or del NS1 virus. At 24 and 48 h post infection, the cells were subjected to indirect immunofluorescence assays with anti-ASC and anti-cleaved caspase-3 antibodies. The average number of cleaved caspase-3-positive and ASC speck-positive cells and standard deviations obtained from three independent experiments are shown ($n > 100$). **$P < 0.01$ by Student's t test.

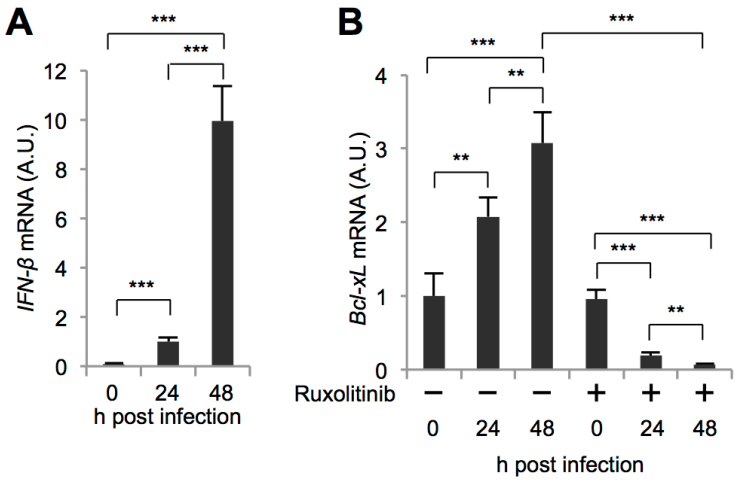

Figure 10 Induced expression of Bcl-xL by JAK-STAT pathway antagonizes proapoptotic Bcl-2 family proteins to inhibit the apoptotic cell death in infected PL16T cells.

(A) PL16T cells were infected with wild-type IAV. At 24 and 48 h post infection, cells were collected and the total RNAs were subjected to reverse transcription followed by real-time PCR with primers specific for *IFN-β* mRNA. The mean value and standard deviations obtained from three independent experiments are shown. (B) PL16T cells were infected with wild-type IAV in the absence or presence of 1 μg/ml ruxolitinib. At 24 and 48 h post infection, total RNAs were purified and were subjected to reverse transcription followed by real-time PCR with primers specific for *Bcl-xL* mRNA. The mean value and standard deviations obtained from three independent experiments are shown. **P < 0.01, ***P < 0.001 by Student's t test.

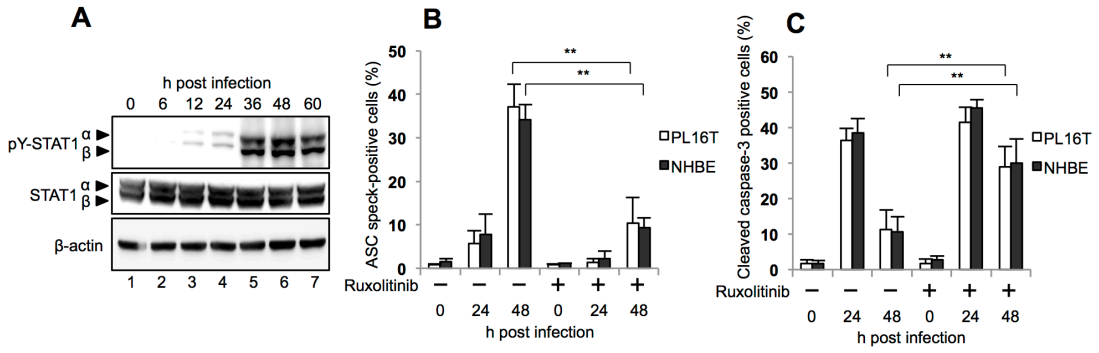

Figure 11 Type I IFN triggers pyroptosis but not apoptosis in a mutually exclusive manner.

(A) At 0, 6, 12, 24, 36, 48, and 60 h post infection, infected PL16T cells were lysed, and the cell lysates were subjected to western blot analysis using anti-phospho-STAT1 (Tyr701) and STAT1. β-actin was detected as a loading control. (B and C) PL16T and NHBE cells were infected with IAV at MOI of 10 in the absence or presence of 1 μg/ml Ruxolitinib. At 24 and 48 h post infection, PL16T and NHBE cells were subjected to indirect immunofluorescence assays using anti-cleaved caspase-3 and anti-ASC antibodies. Percent of cleaved caspase-3-positive cells (B) and ASC speck-positive cells (C) were quantified. The data represent averages with standard deviations from three independent experiments (n > 100).

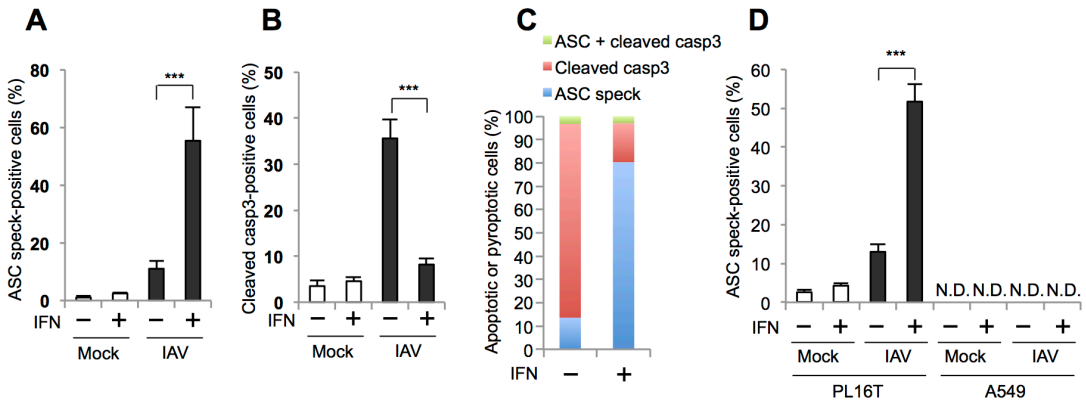

Figure 12 Type I IFN signaling pathway is responsible for switching cell death pathway from apoptosis to pyroptosis in infected respiratory epithelial cells.

(A to C) At 6 h post infection, infected PL16T cells were incubated with or without 1,000 IU/ml IFN-β. At 24 h post infection, cells were subjected to indirect immunofluorescence assays using anti-ASC and anti-cleaved caspase-3 antibodies. The average number of ASC speck-positive (A) and cleaved caspase-3-positive (B) cells and standard deviations obtained from three independent experiments are shown (n > 100). The percentage of ASC speck-positive (blue), cleaved caspase-3-positive (red), and cleaved caspase-3/ASC speck-positive cells (green) are counted (C). (D) At 6 h post infection, infected PL16T and A549 cells were incubated with or without 1,000 IU/ml IFN-β. At 24 h post infection, cells were subjected to indirect immunofluorescence assays using anti-ASC antibody. The average number of ASC speck-positive cells and standard deviations obtained from three independent experiments are shown (n > 100). **P < 0.01, ***P < 0.001 by Student's t test. N.D., not detected.

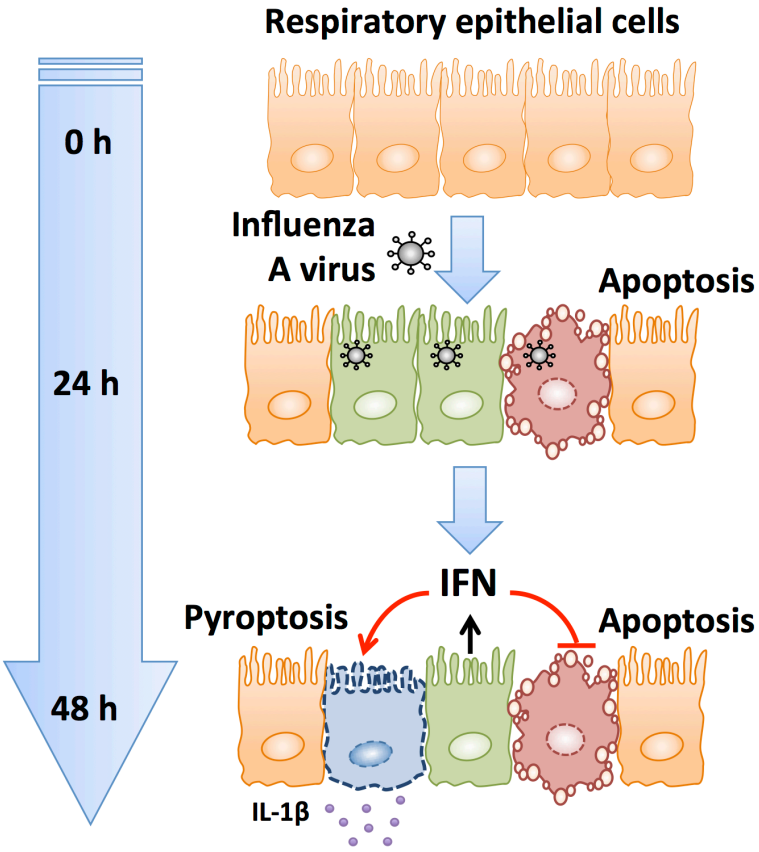

Figure 13 Model: type I IFN signaling pathway triggers pyroptosis but not apoptosis in the respiratory epithelial cells in a mutually exclusive manner.

Apoptosis is induced at early phases of infection, but the cell death pathway is shifted to pyroptosis at late phases of infection under the regulation of type I IFN signaling to promote pro-inflammatory cytokines production.

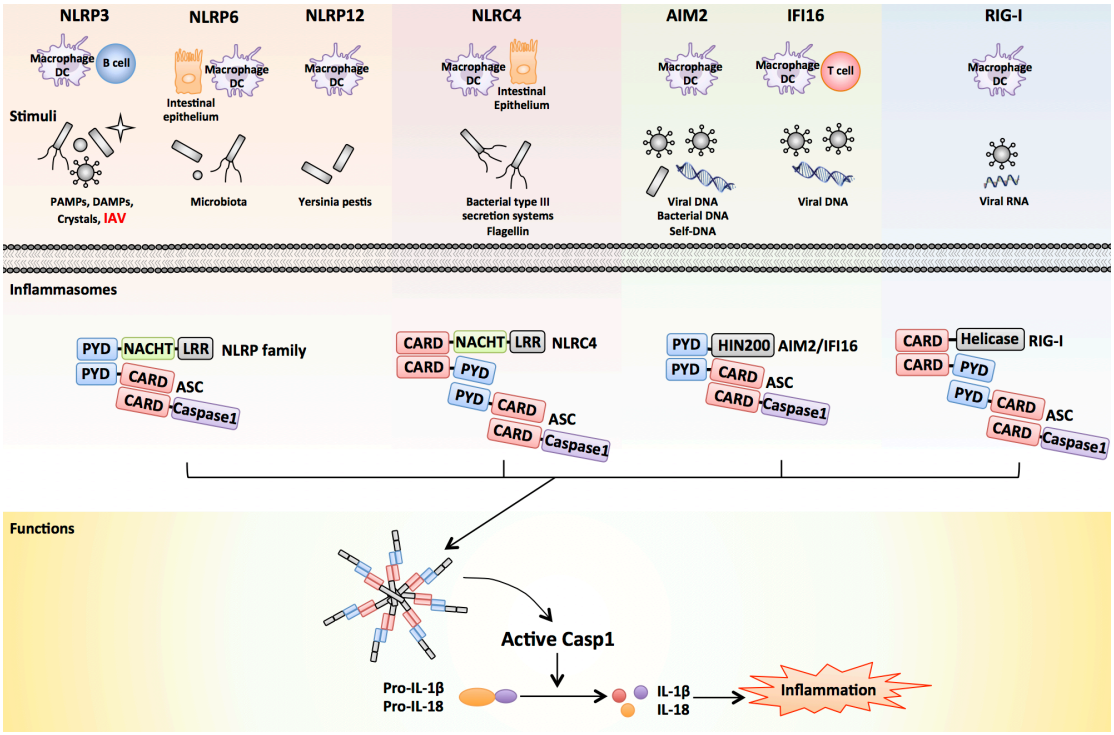

Figure 14 Overviews of various inflammasome receptor induced by a variety of stimuli.

Inflammasome assembly can be triggered by sensing of a variety of stimuli that are associated with infection or cellular stress and culminates in the activation of caspase-1. DC, dendritic cell.

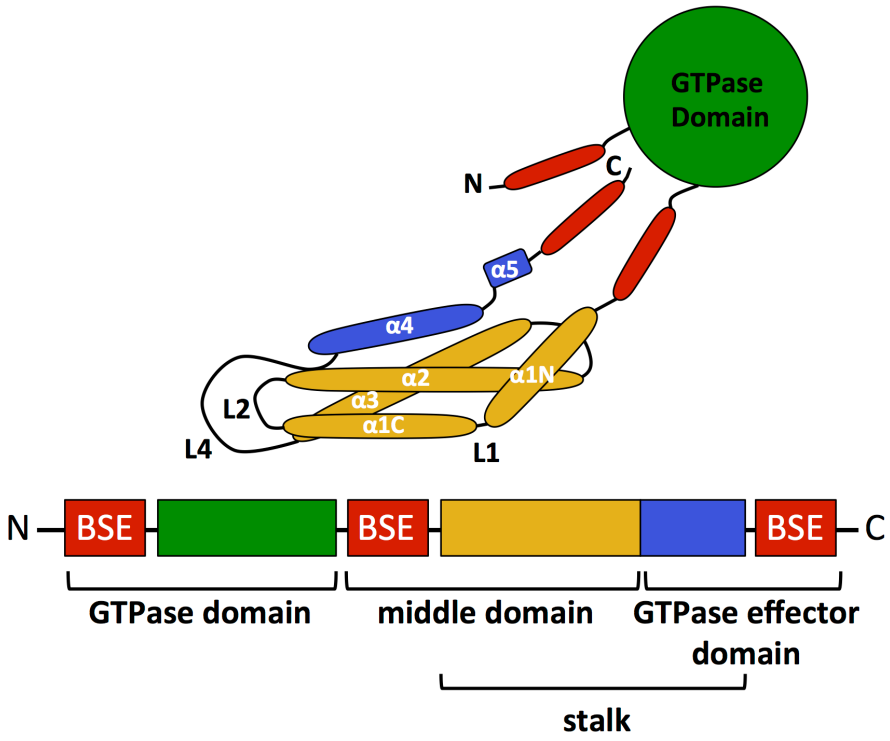

Figure 15 Domain structure of human MxA.

Human MxA consists of N-terminal GTPase domain, central middle domain, and C-terminal GTPase effector domain. GTPase domain is connected to an elongated stalk that consists of a four-helix bundle comprising the middle domain and GTPase effector domain. The connection between the GTPase domain and the stalk consists of a bundle signaling element (BSE).

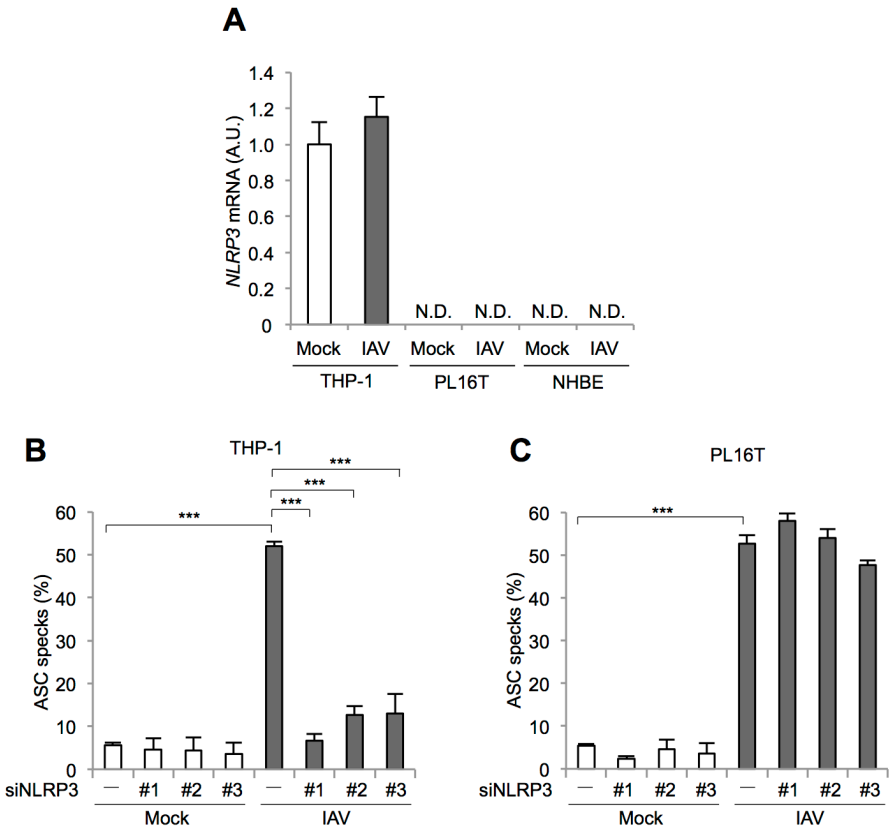

Figure 16 NLRP3 does not promote inflammasome assembly in respiratory epithelial cells against IAV infection.

(A) At 36 h post infection, total RNAs were purified from uninfected and infected THP-1, PL16T, and NHBE cells, and subjected to real-time PCR with primers specific for *Nlrp3* mRNA. The mean value and standard deviations obtained from three independent experiments are shown. N.D., not detected. (B and C) FLAG-GFP-ASC-THP-1 (B) or FLAG-GFP-ASC PL16T (C) cells were transfected with either non-targeting or NLRP3 targeting siRNA. At 48 h post transfection, the cells were infected with IAV and measured ASC specks by ArrayScan^{TM} high-content systems. #1, #2, #3 indicate different sequences of either NLRP3 siRNA. The average number of ASC speck-positive cells and standard deviations obtained from three independent experiments are shown ($n > 100$). ***$P < 0.001$ by Student's t test.

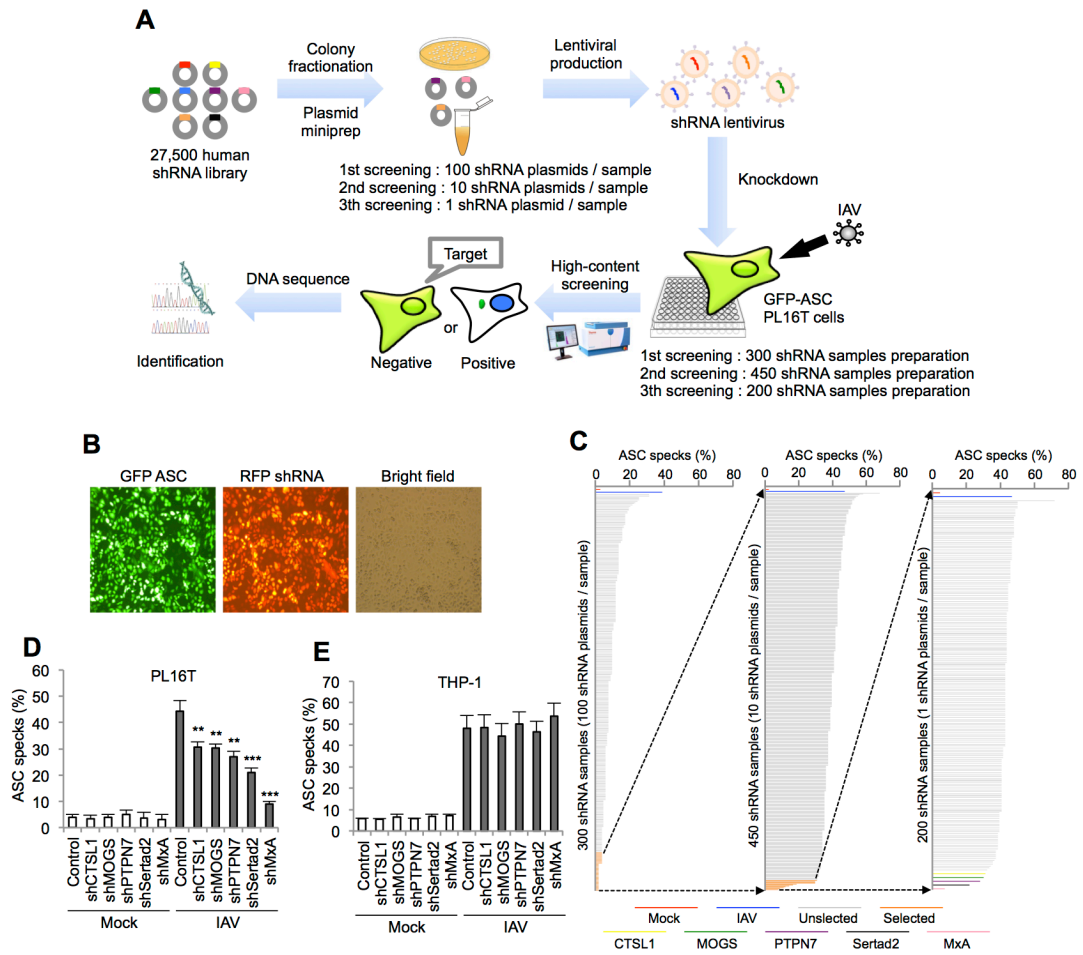

Figure 17 High-content lentiviral shRNA screening.

(A) Overview of high-content lentiviral shRNA screening workflow. (B) The representative result of lentiviral transduction efficiency of FLAG-GFP-ASC and RFP shRNA in PL16T cells. (C to E) High-content lentiviral shRNA screening of ASC specks induced by IAV infection (MOI = 10) using FLAG-GFP-ASC PL16T cells (C) and the ASC specks quantification with shRNA targeting genes in FLAG-GFP-ASC PL16T (D) and FLAG-GFP-ASC THP-1 cells (E). The data represent averages with standard deviations from three independent experiments (n > 100). **P < 0.01; ***P < 0.001 by Student's t test (versus control IAV infection).

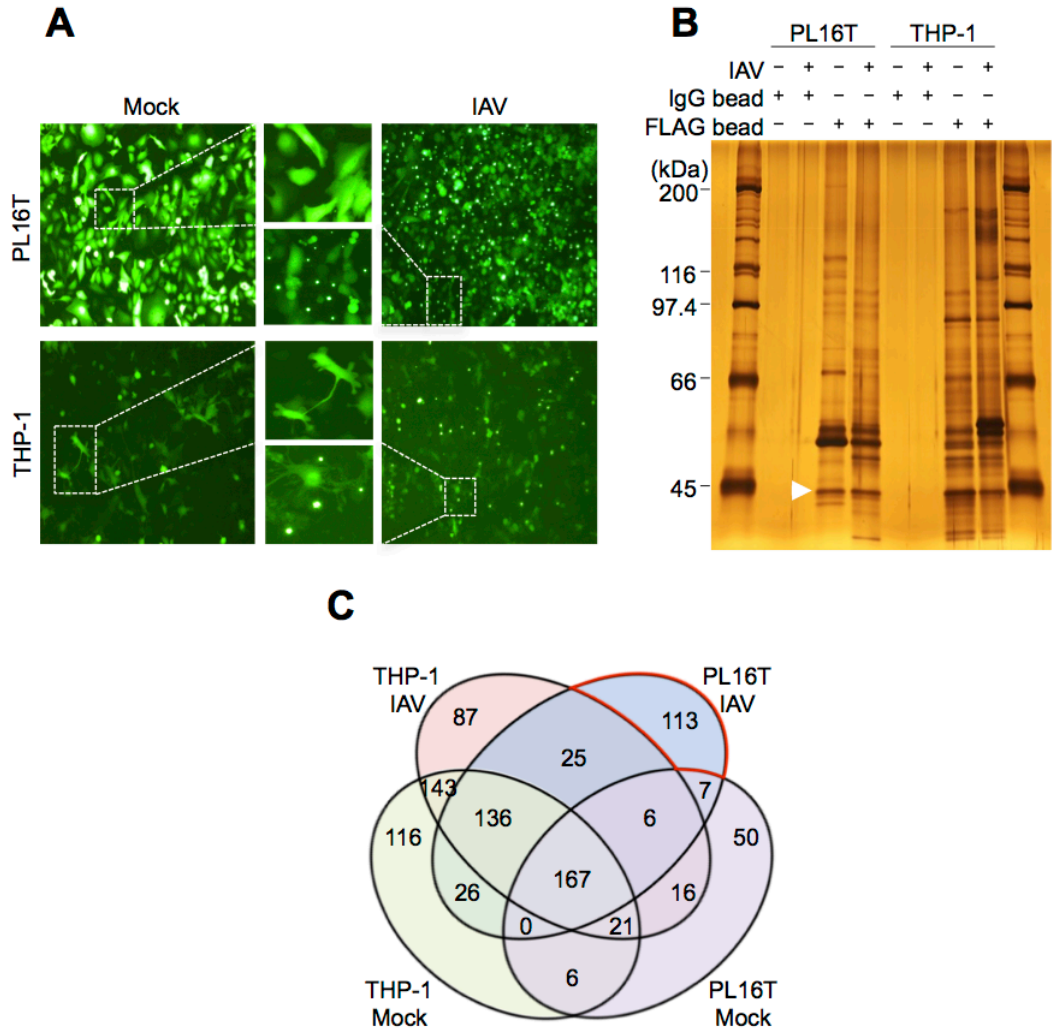

Figure 18 Proteomic approach of ASC interacting proteins.

(A and B) Representative fluorescence images of FLAG-GFP-ASC PL16T and FLAG-GFP-ASC THP-1 cells at 36 h post infection (A) and the cell lysates were subjected to immunoprecipitation with anti-FLAG antibodies-conjugated beads and SDS-PAGE for silver staining (B). Arrowhead indicates FLAG-GFP-ASC. (C) Venn diagram of mass spectrometry data analysis of ASC interacting proteins. Numbers indicate numbers of the interacting partner of ASC.

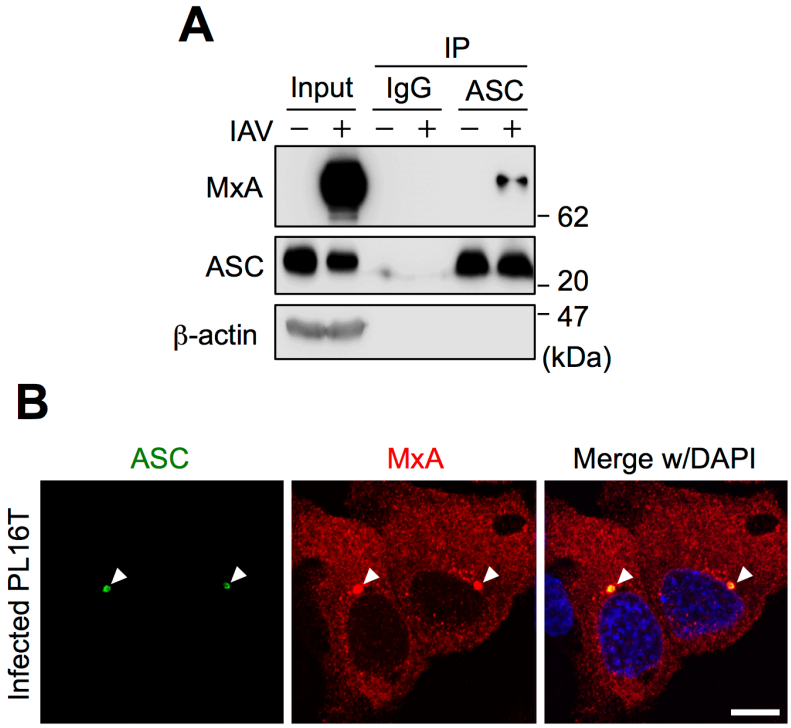

Figure 19 MxA interacts with ASC in respiratory epithelial cells against IAV infection.

(A) At 48 h post infection, PL16T cell lysates were immunoprecipitated with anti-ASC antibody and subjected to western blot analysis with indicated antibodies. (B) At 48 h post infection, PL16T cells were subjected to indirect immunofluorescence assays with anti-ASC (green) and anti-MxA (red) antibodies. Arrowhead indicates intracellular inflammasome localization of the endogenous ASC and MxA. Scale bar, 5 μm. Results are representative of two independent experiments.

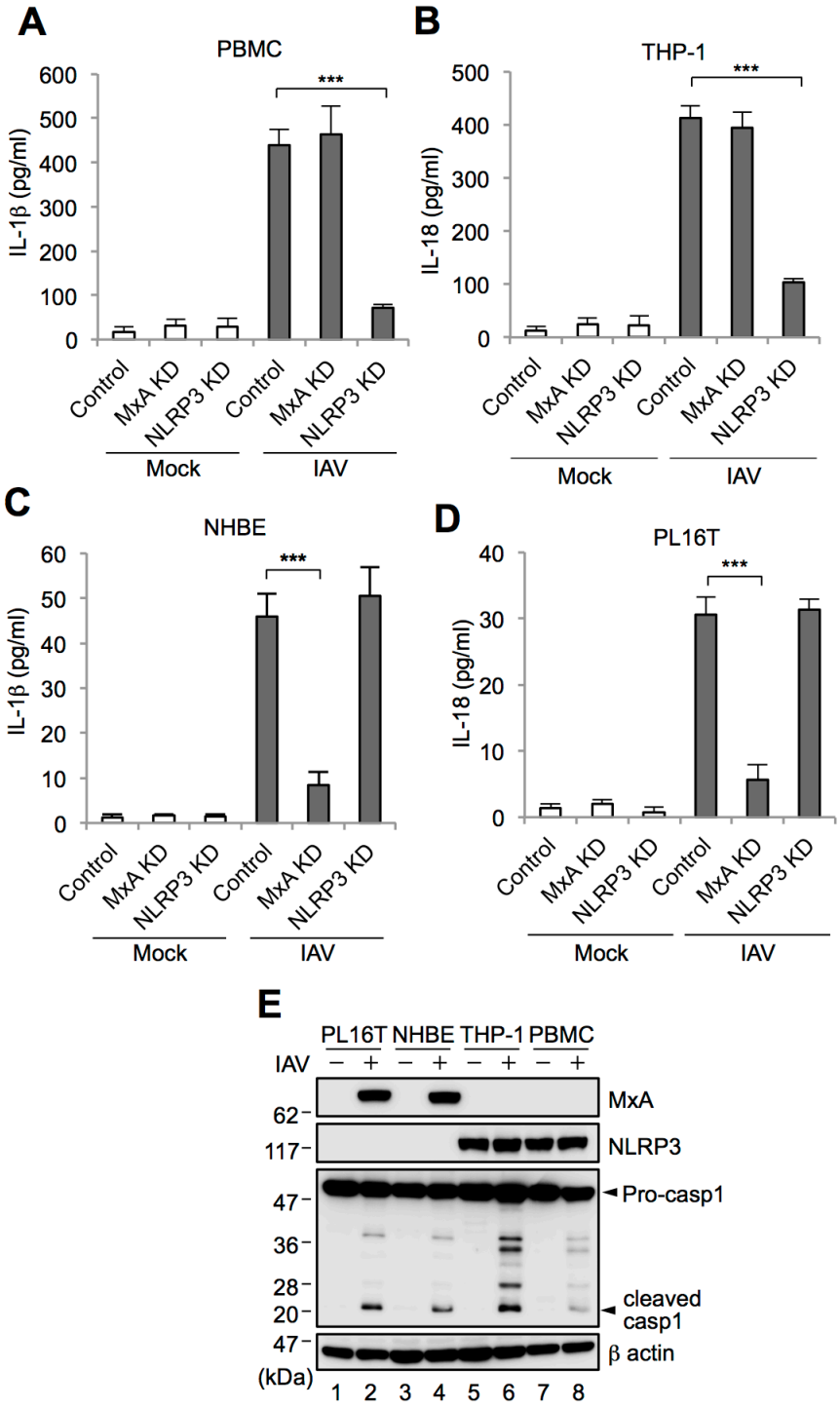
A
PBMC
IL-1β (pg/ml)
600
500
400
300
200
100
0
***
Control
MxA KD
NLRP3 KD
Control
MxA KD
NLRP3 KD
Mock
IAV
B
THP-1
IL-18 (pg/ml)
500
400
300
200
100
0
***
Control
MxA KD
NLRP3 KD
Control
MxA KD
NLRP3 KD
Mock
IAV
C
NHBE
IL-1β (pg/ml)
60
50
40
30
20
10
0
***
Control
MxA KD
NLRP3 KD
Control
MxA KD
NLRP3 KD
Mock
IAV
D
PL16T
IL-18 (pg/ml)
40
30
20
10
0
***
Control
MxA KD
NLRP3 KD
Control
MxA KD
NLRP3 KD
Mock
IAV
E
PL16T NHBE THP-1 PBMC
IAV − + − + − + − +
62
117
47
36
28
20
47
(kDa)
MxA
NLRP3
Pro-casp1
cleaved casp1
β actin
1 2 3 4 5 6 7 8

Figure 20 MxA knockdown specifically abrogates IL-1β and IL-18 secretion in respiratory epithelial cells to viral infection.

(A to D) At 48 h post transfection with either non-targeting, MxA, or NLRP3 siRNA, PBMC-derived macrophages, THP-1, NHBE, or PL16T cells were infected with IAV at MOI of 10. IL-1β secretion in PBMC-derived macrophages (A) and NHBE cells (C), and IL-18 secretion in THP-1 (B) and PL16T cells (D) were measured by ELISA. KD, knockdown. The data represent averages with standard deviations from three independent experiments ($n > 100$). ***$P < 0.001$ by Student's t test. (E) At 48 h post infection, uninfected and infected cells were subjected to western blot analysis with anti-MxA, anti-NLRP3, and anti-caspase-1 antibodies. β-actin was detected as a loading control. Result is representative of two independent experiments.

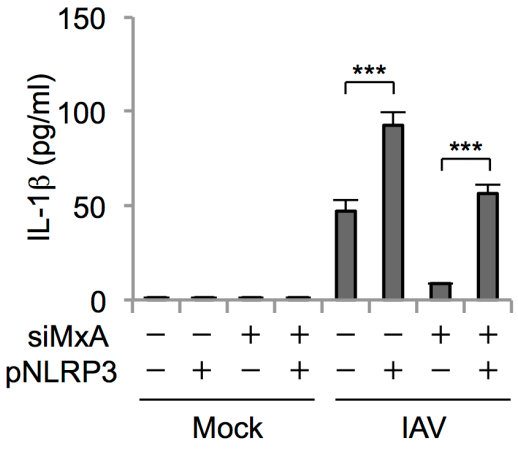

Figure 21 NLRP3 overexpression rescued IL-1β secretion after knockdown of MxA in respiratory epithelial cells.

Lentiviral empty or NLRP3 transduced PL16T cells were transfected with either non-targeting or MxA siRNA and quantified IL-1β release at 72 h post infection. The data represent averages with standard deviations from three independent experiments ($n > 100$). ***$P < 0.001$ by Student's t test.

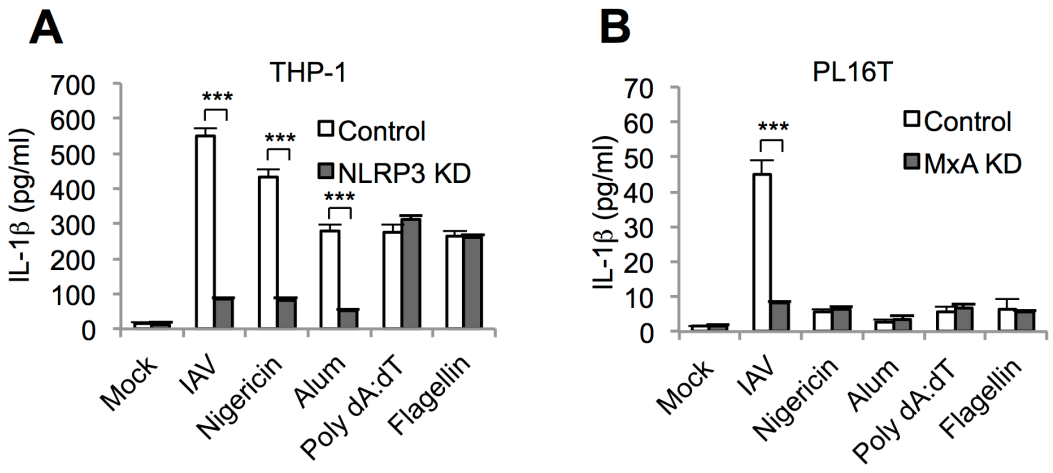

Figure 22 Various stimuli to other inflammasome receptors do not induce MxA inflammasome in respiratory epithelial cells.

(A and B) IL-1β release was measured in 200 ng/ml LPS primed NLRP3 knockdown THP-1 (A) or MxA knockdown PL16T cells (B) with IAV infection at MOI of 10, 5 μg/ml nigericin, 250 μg/ml alum, 3 μg/ml poly(dA:dT), or 500 ng/ml flagellin. Mock represents the cells primed with 200 ng/ml LPS without further stimulation. The data represent averages with standard deviations from three independent experiments ($n > 100$). ***$P < 0.001$ by Student's t test.

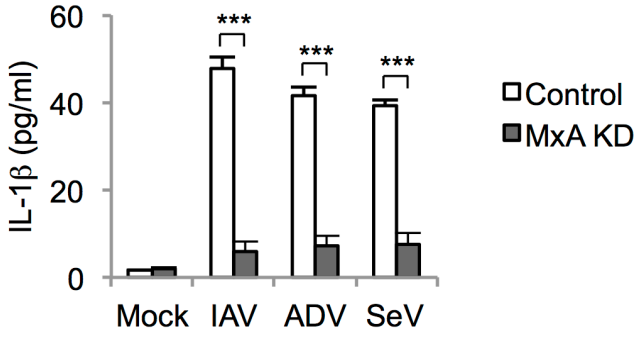

Figure 23 Infection of adenovirus and sendai virus stimulates MxA inflammasome in respiratory epithelial cells.

After transfection with non-targeting or MxA siRNA, PL16T cells were infected with IAV, ADV, or SeV at MOI of 10 and measured IL-1β secretion at 72 h post infection. The data represent averages with standard deviations from three independent experiments ($n > 100$). ***$P < 0.001$ by Student's t test.

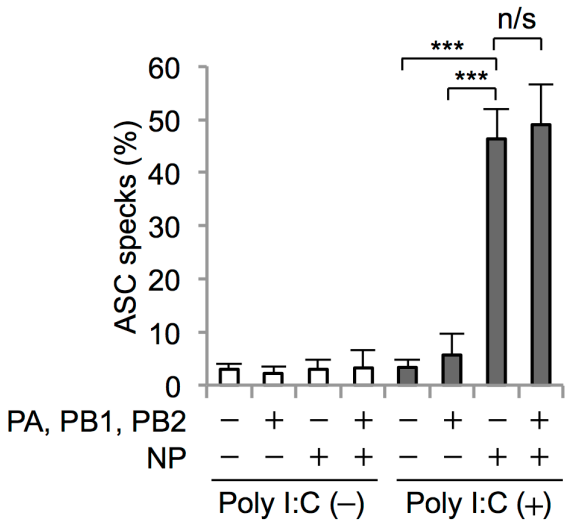

Figure 24 Viral protein NP functions as a ligand of MxA inflammasome in respiratory epithelial cells.

At 24 h post transfection of empty, PA, PB1, PB2, and NP plasmid, poly I:C was treated. ASC specks were quantified by ArrayScan^{TM} high-content systems. The data represent averages with standard deviations from three independent experiments (n > 100). ***P < 0.001 by Student's t test.

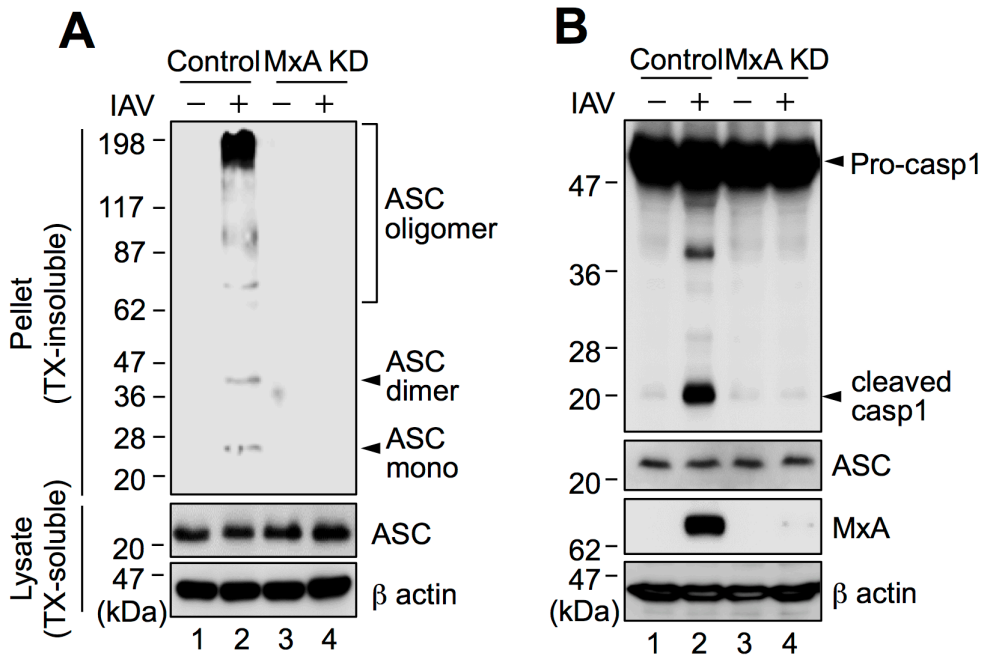

Figure 25 MxA knockdown diminishes ASC oligomerization and activation of caspase-1 in respiratory epithelial cells against viral infection.

(A and B) After transfection with either non-target or MxA siRNA in PL16T cells, ASC oligomerization assay was performed at 48 h post IAV infection (A) or cell lysates were subjected to western blot analysis with the indicated antibodies (B). TX, Triton X-100. Results are representative of two independent experiments.

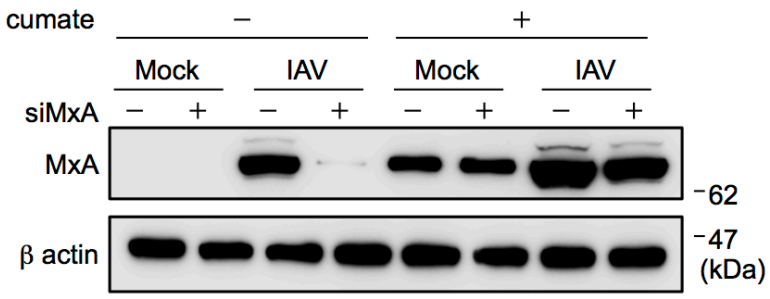

Figure 26 Expression of siRNA-resistant MxA allowed to rescue the reduction of MxA expression

Using lentiviral SparQ cumate switch system, siRNA resistant MxA was expressed in PL16T cells. After transfection with either non-target or MxA siRNA, the cells were infected with IAV infection and added cumate to MxA switch on at 6 h post infection. At 36 h post infection, cell lysates subjected to western blot analysis with the indicated antibodies. Results are representative of two independent experiments.

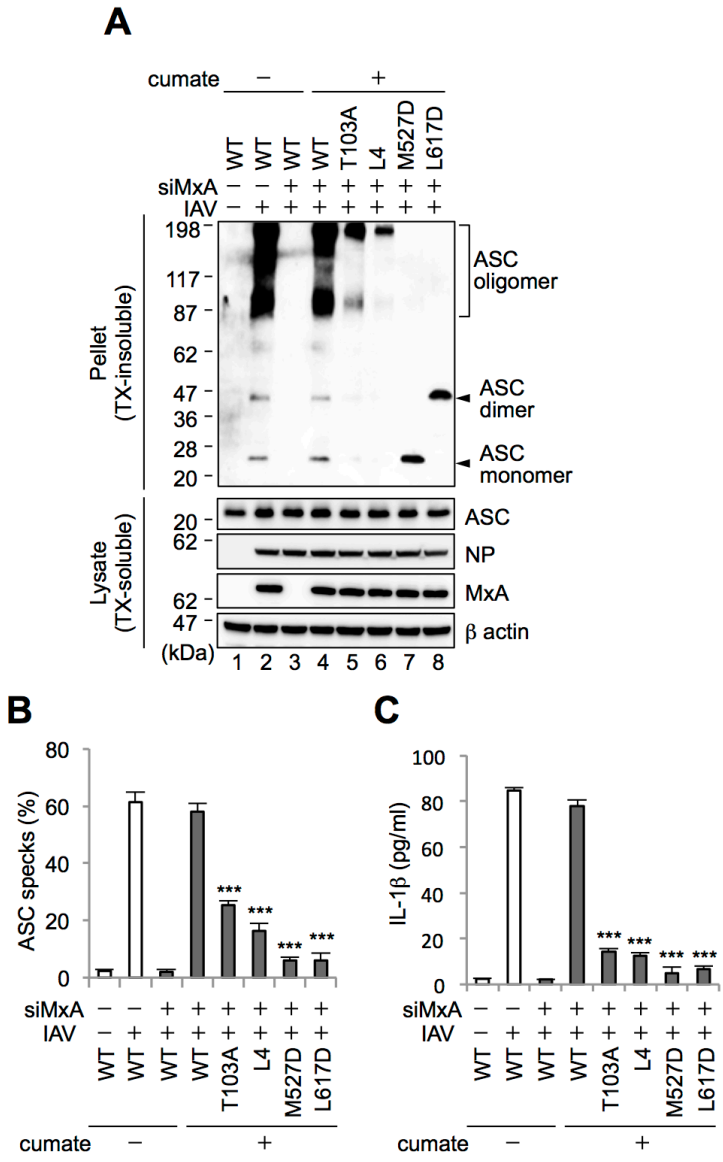

Figure 27 Oligomerization of MxA is required for the inflammasome formation in respiratory epithelial cells.

(A to C) siRNA-resistant MxA mutant including wild-type (WT), T103A, K554E to K557E (L4), M527D, or L617D was expressed in PL16T cells. After transfection with either non-target or MxA siRNA, the cells were infected with IAV and ASC oligomerization (A), ASC specks (B), and IL-1β release (C) were measured. Result is representative of two independent experiments (A) and the data represent averages with standard deviations from three independent experiments (n > 100) (B, C). ***P < 0.001 by Student's t test (versus lane 4).

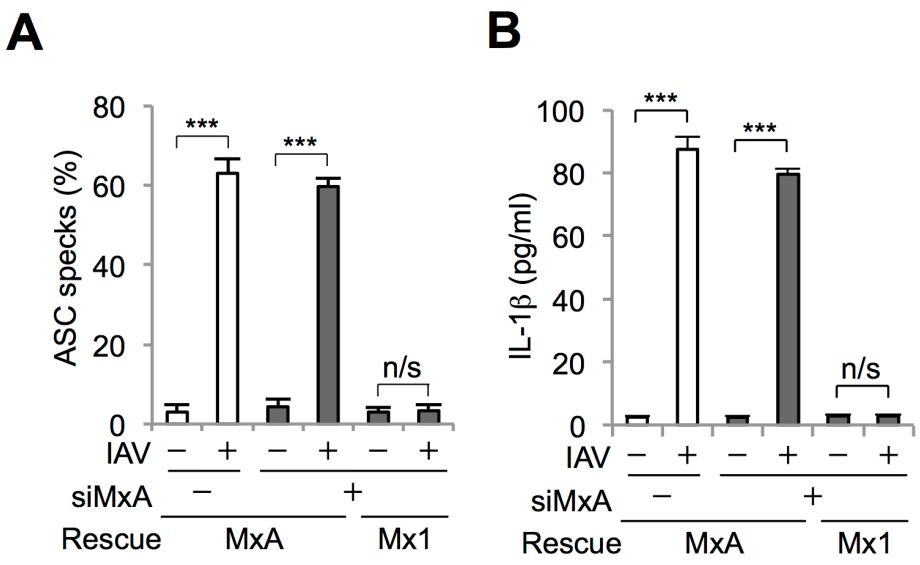

Figure 28 Nuclear localized mouse Mx1 is not responsible for inflammasome in respiratory epithelial cells against IAV infection.

(A and B) Using lentiviral SparQ cumate switch system, mouse Mx1 was expressed in PL16T cells. After transfection with either non-target or MxA siRNA, the cells were infected with IAV and ASC specks (A), and IL-1β release (B) were measured. n/s, not significant. The data represent averages with standard deviations from three independent experiments (n > 100). ***P < 0.001 by Student's t test.

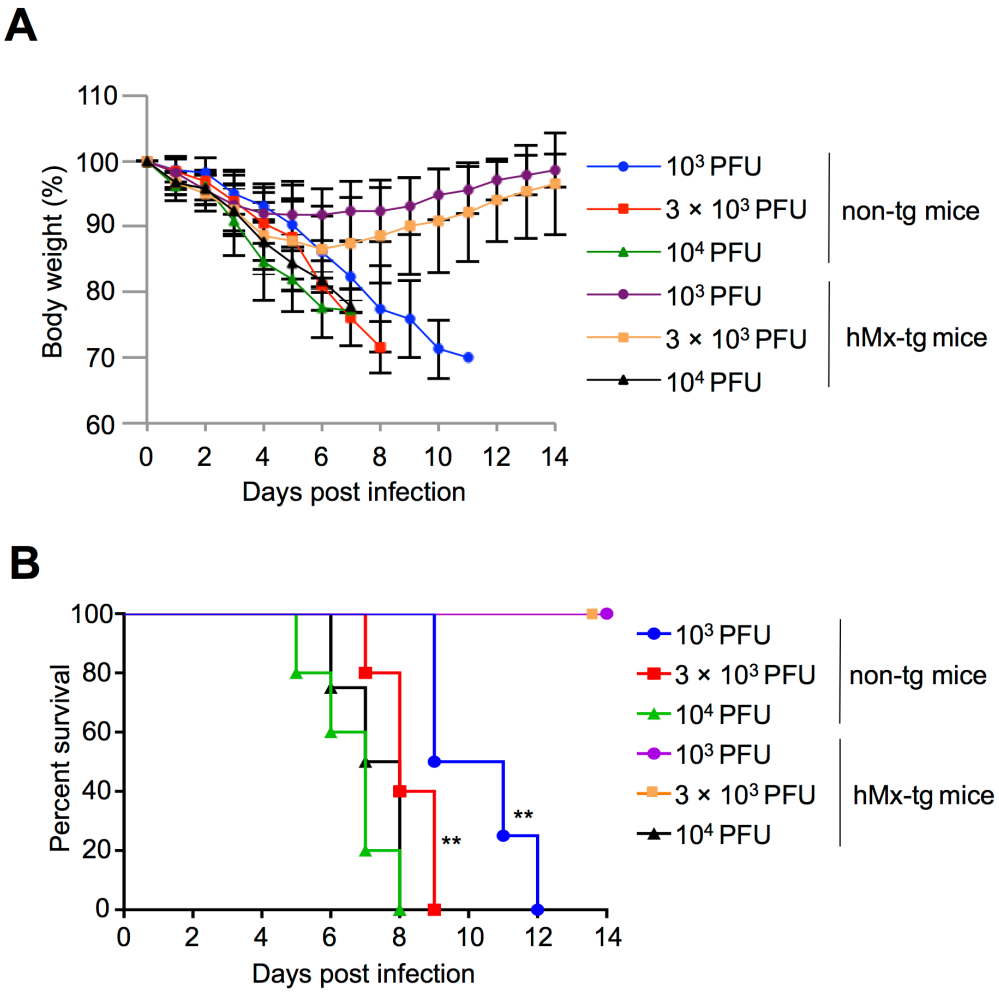

Figure 29 hMx-tg mice confer high resistance to IAV infection.

(A and B) Non-tg and hMx-tg mice were infected intranasally with the indicated doses of IAV. Weight loss (A) and survival (B) were monitored for 14 days (n = 4 to 5 mice per group, n = 2 mice per naïve group). The data represent averages with standard deviations (A) and results are combined from two independent experiments (A, B). ** $p<0.01$ (non-tg 10^3 PFU versus hMx-tg 10^3 PFU, non-tg 3×10^3 PFU versus hMx-tg 3×10^3 PFU) by Log-rank (Mantel-Cox).

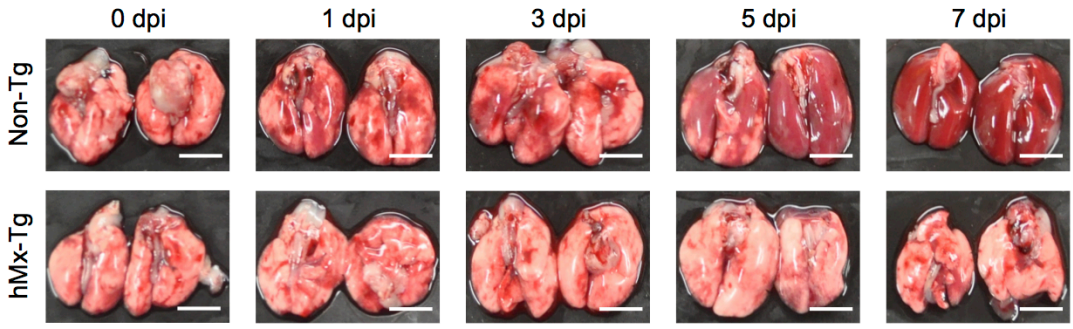

Figure 30 The lung macroscopic lesions of hMx-Tg mice.

Non-Tg and hMx-Tg mice were infected with 3,000 PFU of IAV. At the indicated days post infection (dpi), the lung gross appearance was monitored (n = 2 mice per group at each day). Scale bar, 5 mm.

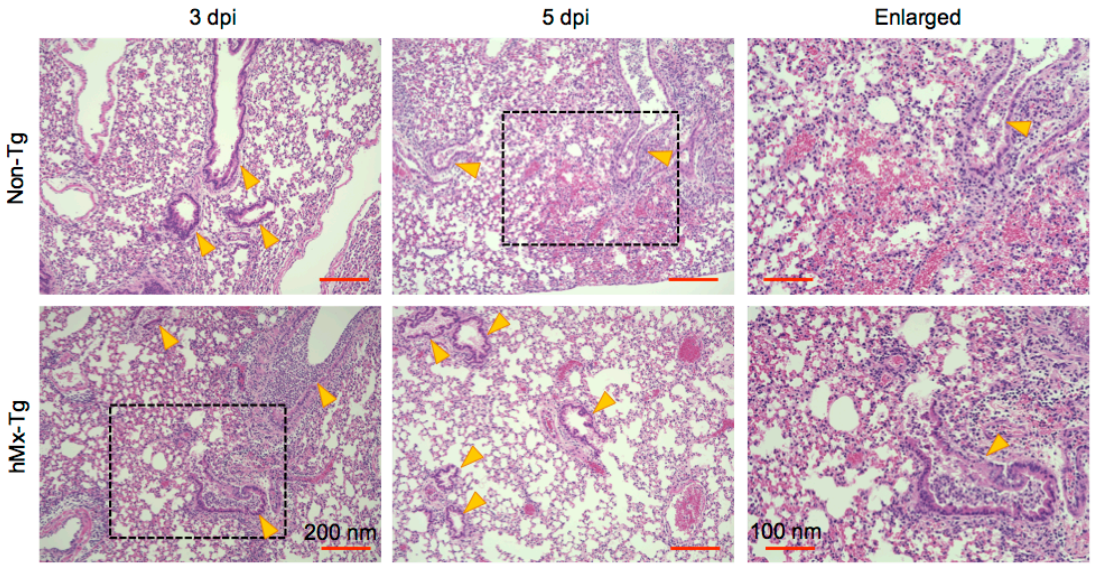

Figure 31 Leukocytes in hMx-tg mice migrate into the bronchioles to remove IAV at the early phage of viral infection.

Non-tg and hMx-tg mice were infected intranasally with 3×10^3 PFU of IAV. At indicated days post infection (dpi), the lung tissue sections were stained with hematoxylin and eosin. Arrowheads indicate bronchioles. Result is representative of two independent experiments.

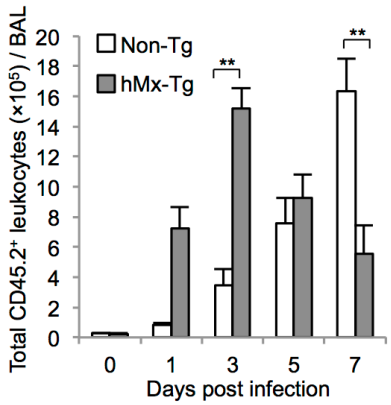

Figure 32 Robust total leukocyte recruitment in hMx-tg mice at early phases of viral infection.

Non-tg and hMx-tg mice were infected intranasally with 3×10^3 PFU of IAV. At indicated days post infection, BAL was collected by washing the trachea and lungs twice by injecting a total of 2 ml PBS containing 0.1% BSA and measured $CD45.2^+$ total BAL leukocytes by flow cytometry. n = 3 mice per group. The data represent averages with standard deviations from two independent experiments (n > 100). **P < 0.01 by Student's t test.

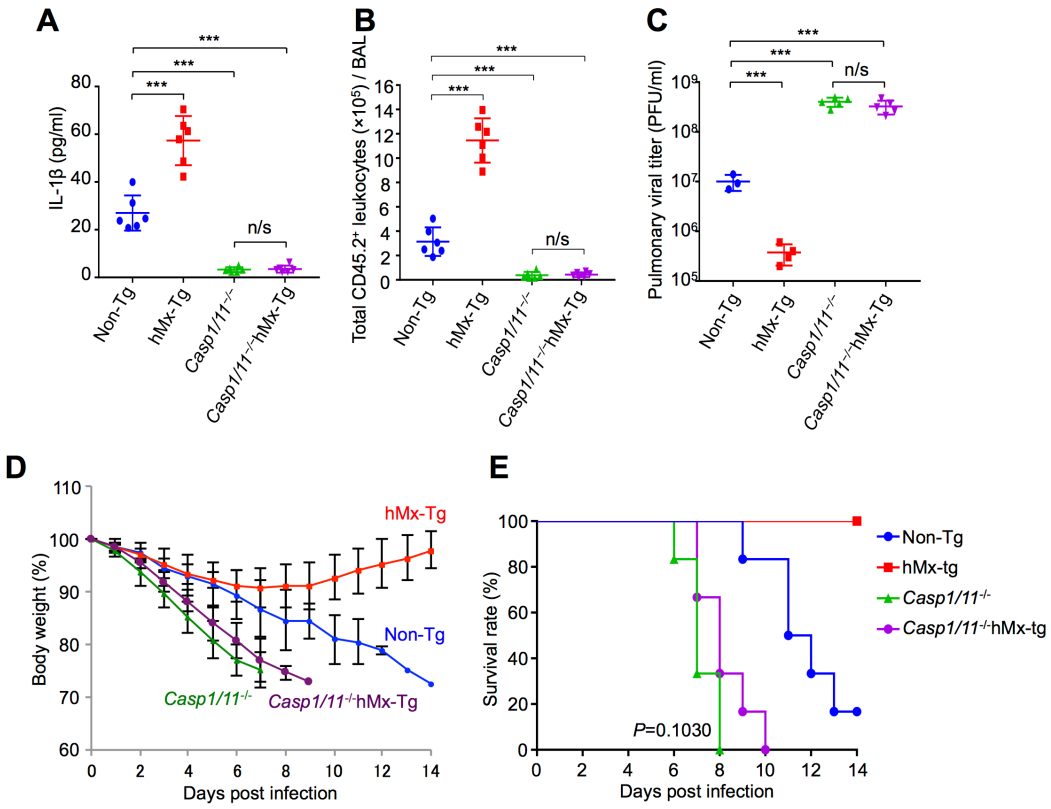

Figure 33 ***Casp1/11*$^{-/-}$ × hMx-tg mice results in comparable susceptibility with *Casp1/11*$^{-/-}$ mice against IAV infection.**

(A and C) Indicated group of mice was infected intranasally with 3 × 10^3 PFU of IAV. At 3 days post infection, BAL was collected and measured IL-1β release (A) or CD45.2$^+$ total BAL leukocytes (B). At 5 days post infection, lung homogenate was prepared in 2 ml PBS and tissue-free supernatant was subjected to plaque assay (C). Each symbol represents one mouse. n = 2 mice per naïve group. n/s, not significant. mean ± s.e.m., ***P < 0.001 by Student's t test. (D and E) Indicated group of mice was infected intranasally with 10^3 PFU of IAV. Weight loss (D) and survival (E) were monitored for 14 days (n = 6 mice per group, n = 2 mice per naïve group). P = 0.1030 (*Casp1/11*$^{-/-}$ versus *Casp1/11*$^{-/-}$ × hMx-tg) by Log-rank (Mantel-Cox). Results are combined from two independent experiments.

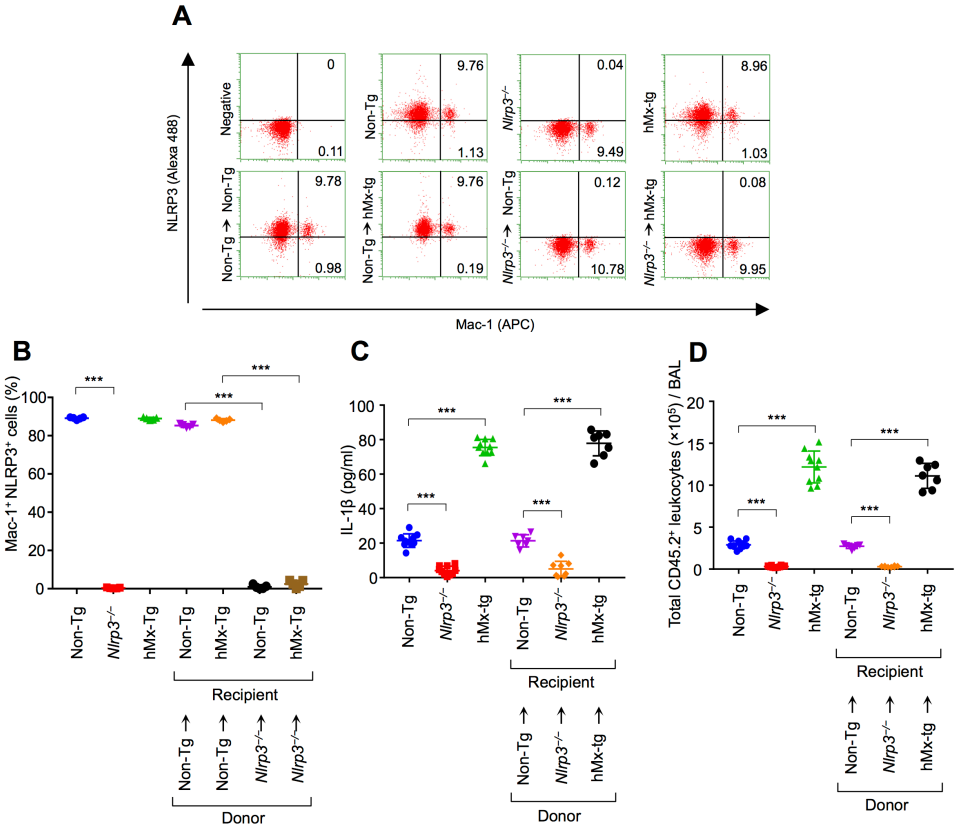

Figure 34 Confirmation of engraftment of bone marrow transplantation.

(A and B) The indicated group of mice were infected intranasally with 3×10^3 PFU of IAV. At 3 days post infection, the cells were collected from bone marrow. Representative flow cytometric analysis of $CD11b^+$ (mac-1) and $NLRP3^+$ cells in bone marrow (A). Numbers indicate the percentage of gated populations. Negative indicates staining with control IgG antibodies. The percentage of $CD11b^+$ (mac-1) and $NLRP3^+$ cells in bone marrow by flow cytometry (B). (C and D) The indicated group of mice were infected intranasally with 3×10^3 PFU of IAV. At 3 days post infection, BAL was collected and measured IL-1β release (C) or total BAL leukocytes (D). Each symbol represents one mouse. n = 2 mice per naïve group. mean ± s.e.m., ***P < 0.001 by Student's t test. Results are combined from two independent experiments.

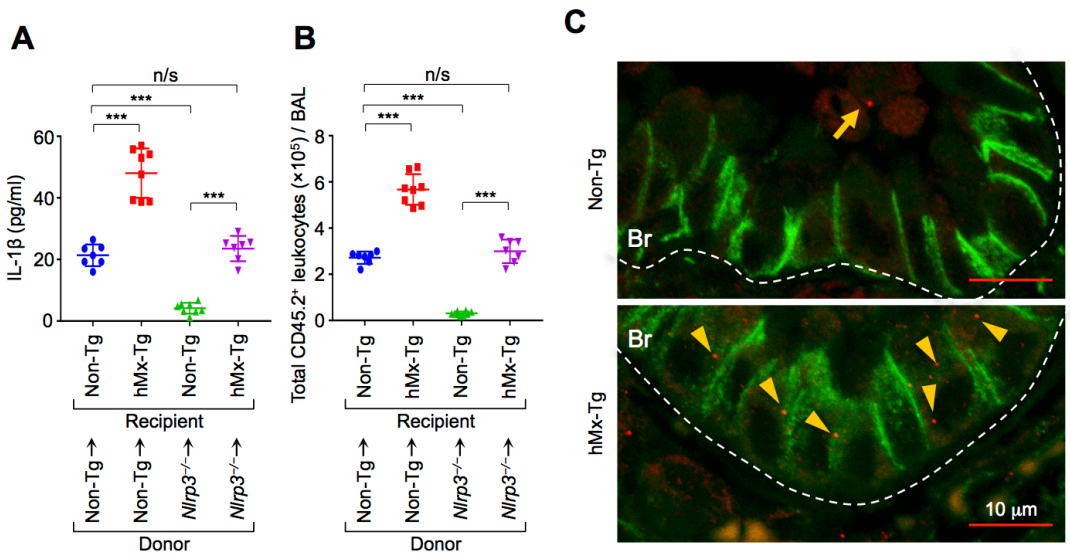

Figure 35 MxA is required for the inflammasome activation in respiratory epithelial cells *in vivo*.

(A and B) The indicated group of mice were infected intranasally with 3×10^3 PFU of IAV. At 3 days post infection, BAL was collected and measured IL-1β release (A) or total BAL leukocytes (B). Each symbol represents one mouse. n = 2 mice per naïve group. n/s, not significant. mean ± s.e.m., ***P < 0.001 by Student's t test. Results are combined from two independent experiments. (C) At 3 days post infection, lung tissue sections were subjected to indirect immunofluorescence assays with anti-β-catenin (green) and anti-ASC (red) antibodies. ASC specks in epithelial cells (arrowheads) and in immune cells (arrow) are indicated. Br, bronchioles. Result is representative of two independent experiments.

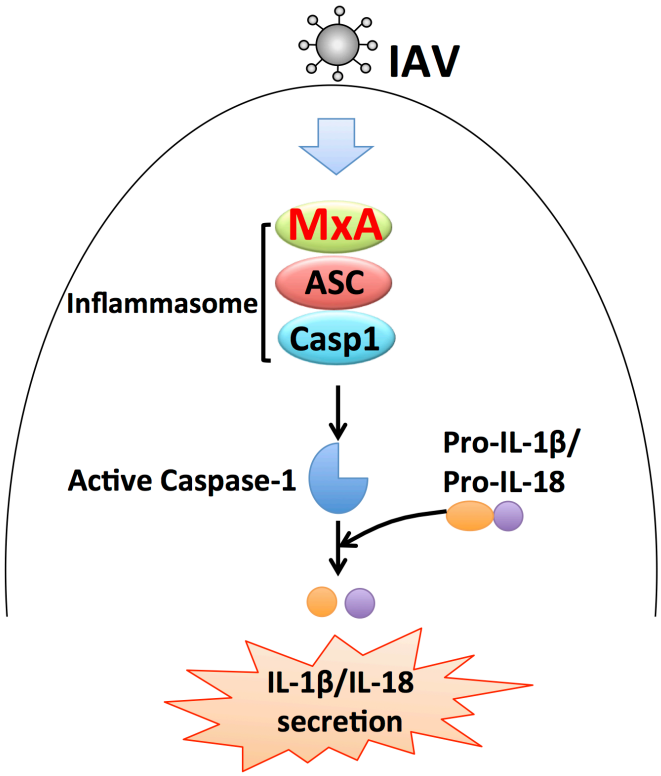

Figure 36 Model: MxA selectively functions as an inflammasome sensor in respiratory epithelial cells against influenza virus infection.

MxA in respiratory epithelial cells selectively forms inflammasome complexes with the ASC and caspase-1 to promote IL-1β and IL-18 secretion against IAV infection.

Acknowledgements

I am with you and will watch over you wherever you go.

I will not leave you until I have done what I have promised you.

-Genesis 28 : 15-

I thank God that you are always with me and watch over me wherever I go. You gave me the faith that I surely overcame my difficulties during my Ph.D. program. You showed me your world mission for people who have less fortunate. Heavenly Father, please help me to remember this victory so that I must conquer in Christ no matter how difficult situations I have in the future. AMEN.

I would like to express my deepest thank to professor Kyosuke Nagata who gave me an opportunity to study in his laboratory and expertly guided me during my graduate education and shared the excitement of my five years of research discovery. I sincerely learned from him that what is 'Science' and kept the sentence in my mind forever 'What's new?'.

I sincerely would like to thank to professor Atsushi Kawaguchi who guided me with this research project from the beginning to the end with supports, encouragement, and love. All it took was for me to meet one special teacher like him who believed in me. He taught me to ask good questions, never give up, and never quit learning that I believe these are one of the most important things not only in my Ph.D. program, but also in my whole life.

I am highly obliged in taking instructive comments and research supports to sincerely thanks to Prof. Akira Shibuya, Prof. Yuji Funakoshi, Prof. Yasuyuki Suda, Prof. Tang-Long Shen, Prof. Masayuki Noguchi, Prof. Peter Stäheli, Prof. Kiong Ho, Prof.

Shoko Saito, Ms. Mikako Hirohama, Prof. Takeshi Ichinohe, Dr. Toru Natsume, Dr. Shungo Adachi, Ms. Moe Yamashita, Mr. JinHwan Choi, and Mr. Scott Eisenhower.

I also thank to all of our laboratory members, HBP friends, and SIGMA office members for their warm heart and help many things in my life in Japan.

I especially would like to express my appreciation to Dr. Shuhei Ueshima (Ryu), my best friend, who helped me a lot of my research and private staffs at the beginning of my life in Japan.

I would like to express my special thank to Dr. WooJin Kang and his wife Mrs. KyungOk Nam who fully supported me and my family to adapt well in Japan.

Moreover, I sincerely would like to thank to my former advisor professor Hwajin Park, who gave me high motivation and opportunity to study in Japan.

I next would like to express to my deepest thank to my spiritual mentor, pastor YeonBae Chae, and all my church friends for their prayers and love.

I also would like to express special thank to Mr. JongChan Hwang, Mr. JinHwan Choi, and Mrs. JeongMin Hong for their encouragement and babysitting.

I also would like to express my sincere gratitude to my parent and the parent in law for their unlimited love and financial support.

Finally, I would like to express my deepest appreciation to my wife, Shana YunJung Kim, who loves me, trusts me, and supports me with prayer at every moment. I also would like to express my special thank to my daughter, Samantha SeolA Lee, and my son, Joshua DoHyun Lee, who are the energy of my life.

Frank SangJoon LEE

March 2018

1. Colman PM. 1994. Influenza virus neuraminidase: structure, antibodies, and inhibitors. Protein Sci 3:1687-1696. http://dx.doi.org/10.1002/pro.5560031007.
2. Nobusawa E, Aoyama T, Kato H, Suzuki Y, Tateno Y, Nakajima K. 1991. Comparison of complete amino acid sequences and receptor-binding properties among 13 serotypes of hemagglutinins of influenza A viruses. Virology 182:475-485.
3. Watanabe K, Handa H, Mizumoto K, Nagata K. 1996. Mechanism for inhibition of influenza virus RNA polymerase activity by matrix protein. J Virol 70:241-247.
4. Chan MC, Cheung CY, Chui WH, Tsao SW, Nicholls JM, Chan YO, Chan RW, Long HT, Poon LL, Guan Y, Peiris JS. 2005. Proinflammatory cytokine responses induced by influenza A (H5N1) viruses in primary human alveolar and bronchial epithelial cells. Respir Res 6:135. http://dx.doi.org/10.1186/1465-9921-6-135.
5. Sanders CJ, Doherty PC, Thomas PG. 2011. Respiratory epithelial cells in innate immunity to influenza virus infection. Cell Tissue Res 343:13-21. http://dx.doi.org/10.1007/s00441-010-1043-z.
6. Taubenberger JK, Morens DM. 2006. 1918 Influenza: the mother of all pandemics. Emerg Infect Dis 12:15-22. http://dx.doi.org/10.3201/eid1201.050979.
7. Taubenberger JK, Kash JC. 2010. Influenza virus evolution, host adaptation, and pandemic formation. Cell Host Microbe 7:440-451. http://dx.doi.org/10.1016/j.chom.2010.05.009.

8. Josset L, Zeng H, Kelly SM, Tumpey TM, Katze MG. 2014. Transcriptomic characterization of the novel avian-origin influenza A (H7N9) virus: specific host response and responses intermediate between avian (H5N1 and H7N7) and human (H3N2) viruses and implications for treatment options. MBio 5:e01102-01113. http://dx.doi.org/10.1128/mBio.01102-13.

9. Medina RA, Garcia-Sastre A. 2011. Influenza A viruses: new research developments. Nat Rev Microbiol 9:590-603. http://dx.doi.org/10.1038/nrmicro2613.

10. Barton GM. 2008. A calculated response: control of inflammation by the innate immune system. J Clin Invest 118:413-420. http://dx.doi.org/10.1172/jci34431.

11. Nathan C. 2006. Neutrophils and immunity: challenges and opportunities. Nat Rev Immunol 6:173-182. http://dx.doi.org/10.1038/nri1785.

12. Nathan C. 2002. Points of control in inflammation. Nature 420:846-852. http://dx.doi.org/10.1038/nature01320.

13. Serhan CN, Savill J. 2005. Resolution of inflammation: the beginning programs the end. Nat Immunol 6:1191-1197. http://dx.doi.org/10.1038/ni1276.

14. Drayton DL, Liao S, Mounzer RH, Ruddle NH. 2006. Lymphoid organ development: from ontogeny to neogenesis. Nat Immunol 7:344-353. http://dx.doi.org/10.1038/ni1330.

15. Medzhitov R, Janeway CA, Jr. 1997. Innate immunity: the virtues of a nonclonal system of recognition. Cell 91:295-298.

16. Medzhitov R. 2008. Origin and physiological roles of inflammation. Nature 454:428-435. http://dx.doi.org/10.1038/nature07201.

17. Netea MG, Balkwill F, Chonchol M, Cominelli F, Donath MY, Giamarellos-Bourboulis EJ, Golenbock D, Gresnigt MS, Heneka MT, Hoffman HM, Hotchkiss R, Joosten LAB, Kastner DL, Korte M, Latz E, Libby P, Mandrup-Poulsen T, Mantovani A, Mills KHG, Nowak KL, O'Neill LA, Pickkers P, van der Poll T, Ridker PM, Schalkwijk J, Schwartz DA, Siegmund B, Steer CJ, Tilg H, van der Meer JWM, van de Veerdonk FL, Dinarello CA. 2017. A guiding map for inflammation. Nat Immunol 18:826-831. http://dx.doi.org/10.1038/ni.3790.

18. Scapini P, Marini O, Tecchio C, Cassatella MA. 2016. Human neutrophils in the saga of cellular heterogeneity: insights and open questions. Immunol Rev 273:48-60. http://dx.doi.org/10.1111/imr.12448.

19. Eyerich K, Dimartino V, Cavani A. 2017. IL-17 and IL-22 in immunity: Driving protection and pathology. Eur J Immunol 47:607-614. http://dx.doi.org/10.1002/eji.201646723.

20. Shattuck EC, Muehlenbein MP. 2015. Human sickness behavior: Ultimate and proximate explanations. Am J Phys Anthropol 157:1-18. http://dx.doi.org/10.1002/ajpa.22698.

21. Ward PA. 2010. The harmful role of c5a on innate immunity in sepsis. J Innate Immun 2:439-445. http://dx.doi.org/10.1159/000317194.

22. Turnbull AV, Rivier CL. 1999. Regulation of the hypothalamic-pituitary-adrenal axis by cytokines: actions and mechanisms of action. Physiol Rev 79:1-71. http://dx.doi.org/10.1152/physrev.1999.79.1.1.

23. Fink SL, Cookson BT. 2005. Apoptosis, pyroptosis, and necrosis: mechanistic description of dead and dying eukaryotic cells. Infect Immun 73:1907-1916. http://dx.doi.org/10.1128/iai.73.4.1907-1916.2005.

24. Ashida H, Mimuro H, Ogawa M, Kobayashi T, Sanada T, Kim M, Sasakawa C. 2011. Cell death and infection: a double-edged sword for host and pathogen survival. J Cell Biol 195:931-942. http://dx.doi.org/10.1083/jcb.201108081.

25. Lamkanfi M, Dixit VM. 2010. Manipulation of host cell death pathways during microbial infections. Cell Host Microbe 8:44-54. http://dx.doi.org/10.1016/j.chom.2010.06.007.

26. Creagh EM. 2014. Caspase crosstalk: integration of apoptotic and innate immune signalling pathways. Trends Immunol 35:631-640. http://dx.doi.org/10.1016/j.it.2014.10.004.

27. Cho YS, Challa S, Moquin D, Genga R, Ray TD, Guildford M, Chan FK. 2009. Phosphorylation-driven assembly of the RIP1-RIP3 complex regulates programmed necrosis and virus-induced inflammation. Cell 137:1112-1123. http://dx.doi.org/10.1016/j.cell.2009.05.037.

28. Pirhonen J, Sareneva T, Kurimoto M, Julkunen I, Matikainen S. 1999. Virus infection activates IL-1 beta and IL-18 production in human macrophages by a caspase-1-dependent pathway. J Immunol 162:7322-7329.

29. Kanneganti TD, Body-Malapel M, Amer A, Park JH, Whitfield J, Franchi L, Taraporewala ZF, Miller D, Patton JT, Inohara N, Nunez G. 2006. Critical role for Cryopyrin/Nalp3 in activation of caspase-1 in response to viral infection and double-stranded RNA. J Biol Chem 281:36560-36568. http://dx.doi.org/10.1074/jbc.M607594200.

30. Whitsett JA, Alenghat T. 2015. Respiratory epithelial cells orchestrate pulmonary innate immunity. Nat Immunol 16:27-35. http://dx.doi.org/10.1038/ni.3045.

31. Wurzer WJ, Planz O, Ehrhardt C, Giner M, Silberzahn T, Pleschka S, Ludwig S. 2003. Caspase 3 activation is essential for efficient influenza virus propagation. Embo j 22:2717-2728. http://dx.doi.org/10.1093/emboj/cdg279.

32. Daidoji T, Koma T, Du A, Yang CS, Ueda M, Ikuta K, Nakaya T. 2008. H5N1 avian influenza virus induces apoptotic cell death in mammalian airway epithelial cells. J Virol 82:11294-11307. http://dx.doi.org/10.1128/jvi.01192-08.

33. Takizawa T, Matsukawa S, Higuchi Y, Nakamura S, Nakanishi Y, Fukuda R. 1993. Induction of programmed cell death (apoptosis) by influenza virus infection in tissue culture cells. J Gen Virol 74 (Pt 11):2347-2355. http://dx.doi.org/10.1099/0022-1317-74-11-2347.

34. Feng S, Yang Y, Mei Y, Ma L, Zhu DE, Hoti N, Castanares M, Wu M. 2007. Cleavage of RIP3 inactivates its caspase-independent apoptosis pathway by removal of kinase domain. Cell Signal 19:2056-2067. http://dx.doi.org/10.1016/j.cellsig.2007.05.016.

35. Rebe C, Cathelin S, Launay S, Filomenko R, Prevotat L, L'Ollivier C, Gyan E, Micheau O, Grant S, Dubart-Kupperschmitt A, Fontenay M, Solary E. 2007. Caspase-8 prevents sustained activation of NF-kappaB in monocytes undergoing macrophagic differentiation. Blood 109:1442-1450. http://dx.doi.org/10.1182/blood-2006-03-011585.

36. Zhou R, Yazdi AS, Menu P, Tschopp J. 2011. A role for mitochondria in NLRP3 inflammasome activation. Nature 469:221-225. http://dx.doi.org/10.1038/nature09663.

37. Shimada K, Crother TR, Karlin J, Dagvadorj J, Chiba N, Chen S, Ramanujan VK, Wolf AJ, Vergnes L, Ojcius DM, Rentsendorj A, Vargas M, Guerrero C,

Wang Y, Fitzgerald KA, Underhill DM, Town T, Arditi M. 2012. Oxidized mitochondrial DNA activates the NLRP3 inflammasome during apoptosis. Immunity 36:401-414. http://dx.doi.org/10.1016/j.immuni.2012.01.009.

38. Nakahira K, Haspel JA, Rathinam VA, Lee SJ, Dolinay T, Lam HC, Englert JA, Rabinovitch M, Cernadas M, Kim HP, Fitzgerald KA, Ryter SW, Choi AM. 2011. Autophagy proteins regulate innate immune responses by inhibiting the release of mitochondrial DNA mediated by the NALP3 inflammasome. Nat Immunol 12:222-230. http://dx.doi.org/10.1038/ni.1980.

39. Iyer SS, He Q, Janczy JR, Elliott EI, Zhong Z, Olivier AK, Sadler JJ, Knepper-Adrian V, Han R, Qiao L, Eisenbarth SC, Nauseef WM, Cassel SL, Sutterwala FS. 2013. Mitochondrial cardiolipin is required for Nlrp3 inflammasome activation. Immunity 39:311-323. http://dx.doi.org/10.1016/j.immuni.2013.08.001.

40. Allam R, Lawlor KE, Yu EC, Mildenhall AL, Moujalled DM, Lewis RS, Ke F, Mason KD, White MJ, Stacey KJ, Strasser A, O'Reilly LA, Alexander W, Kile BT, Vaux DL, Vince JE. 2014. Mitochondrial apoptosis is dispensable for NLRP3 inflammasome activation but non-apoptotic caspase-8 is required for inflammasome priming. EMBO Rep 15:982-990. http://dx.doi.org/10.15252/embr.201438463.

41. Subramanian N, Natarajan K, Clatworthy MR, Wang Z, Germain RN. 2013. The adaptor MAVS promotes NLRP3 mitochondrial localization and inflammasome activation. Cell 153:348-361. http://dx.doi.org/10.1016/j.cell.2013.02.054.

42. Chakrabarti A, Banerjee S, Franchi L, Loo YM, Gale M, Jr., Nunez G, Silverman RH. 2015. RNase L activates the NLRP3 inflammasome during

viral infections. Cell Host Microbe 17:466-477. http://dx.doi.org/10.1016/j.chom.2015.02.010.

43. Pothlichet J, Meunier I, Davis BK, Ting JP, Skamene E, von Messling V, Vidal SM. 2013. Type I IFN triggers RIG-I/TLR3/NLRP3-dependent inflammasome activation in influenza A virus infected cells. PLoS Pathog 9:e1003256. http://dx.doi.org/10.1371/journal.ppat.1003256.

44. Guarda G, Braun M, Staehli F, Tardivel A, Mattmann C, Forster I, Farlik M, Decker T, Du Pasquier RA, Romero P, Tschopp J. 2011. Type I interferon inhibits interleukin-1 production and inflammasome activation. Immunity 34:213-223. http://dx.doi.org/10.1016/j.immuni.2011.02.006.

45. Shimada A, Kano J, Ishiyama T, Okubo C, Iijima T, Morishita Y, Minami Y, Inadome Y, Shu Y, Sugita S, Takeuchi T, Noguchi M. 2005. Establishment of an immortalized cell line from a precancerous lesion of lung adenocarcinoma, and genes highly expressed in the early stages of lung adenocarcinoma development. Cancer Sci 96:668-675. http://dx.doi.org/10.1111/j.1349-7006.2005.00100.x.

46. Kawaguchi A, Hirohama M, Harada Y, Osari S, Nagata K. 2015. Influenza Virus Induces Cholesterol-Enriched Endocytic Recycling Compartments for Budozone Formation via Cell Cycle-Independent Centrosome Maturation. PLoS Pathog 11:e1005284. http://dx.doi.org/10.1371/journal.ppat.1005284.

47. Hale BG, Jackson D, Chen YH, Lamb RA, Randall RE. 2006. Influenza A virus NS1 protein binds p85beta and activates phosphatidylinositol-3-kinase signaling. Proc Natl Acad Sci U S A 103:14194-14199. http://dx.doi.org/10.1073/pnas.0606109103.

48. Moriyama M, Chen IY, Kawaguchi A, Koshiba T, Nagata K, Takeyama H, Hasegawa H, Ichinohe T. 2016. The RNA- and TRIM25-Binding Domains of Influenza Virus NS1 Protein Are Essential for Suppression of NLRP3 Inflammasome-Mediated Interleukin-1beta Secretion. J Virol 90:4105-4114. http://dx.doi.org/10.1128/jvi.00120-16.

49. Noguchi M. 2010. Stepwise progression of pulmonary adenocarcinoma--clinical and molecular implications. Cancer Metastasis Rev 29:15-21. http://dx.doi.org/10.1007/s10555-010-9210-y.

50. Liu X, Zhang Z, Ruan J, Pan Y, Magupalli VG, Wu H, Lieberman J. 2016. Inflammasome-activated gasdermin D causes pyroptosis by forming membrane pores. Nature 535:153-158. http://dx.doi.org/10.1038/nature18629.

51. Donelan NR, Basler CF, Garcia-Sastre A. 2003. A recombinant influenza A virus expressing an RNA-binding-defective NS1 protein induces high levels of beta interferon and is attenuated in mice. J Virol 77:13257-13266.

52. Gack MU, Albrecht RA, Urano T, Inn KS, Huang IC, Carnero E, Farzan M, Inoue S, Jung JU, Garcia-Sastre A. 2009. Influenza A virus NS1 targets the ubiquitin ligase TRIM25 to evade recognition by the host viral RNA sensor RIG-I. Cell Host Microbe 5:439-449. http://dx.doi.org/10.1016/j.chom.2009.04.006.

53. Garcia-Sastre A, Egorov A, Matassov D, Brandt S, Levy DE, Durbin JE, Palese P, Muster T. 1998. Influenza A virus lacking the NS1 gene replicates in interferon-deficient systems. Virology 252:324-330.

54. Zha J, Harada H, Yang E, Jockel J, Korsmeyer SJ. 1996. Serine phosphorylation of death agonist BAD in response to survival factor results in binding to 14-3-3 not BCL-X(L). Cell 87:619-628.

55. Datta SR, Dudek H, Tao X, Masters S, Fu H, Gotoh Y, Greenberg ME. 1997. Akt phosphorylation of BAD couples survival signals to the cell-intrinsic death machinery. Cell 91:231-241.

56. Sevilla L, Zaldumbide A, Pognonec P, Boulukos KE. 2001. Transcriptional regulation of the bcl-x gene encoding the anti-apoptotic Bcl-xL protein by Ets, Rel/NFkappaB, STAT and AP1 transcription factor families. Histol Histopathol 16:595-601.

57. Guo G, Marrero L, Rodriguez P, Del Valle L, Ochoa A, Cui Y. 2013. Trp53 inactivation in the tumor microenvironment promotes tumor progression by expanding the immunosuppressive lymphoid-like stromal network. Cancer Res 73:1668-1675. http://dx.doi.org/10.1158/0008-5472.can-12-3810.

58. Crane CA, Panner A, Murray JC, Wilson SP, Xu H, Chen L, Simko JP, Waldman FM, Pieper RO, Parsa AT. 2009. PI(3) kinase is associated with a mechanism of immunoresistance in breast and prostate cancer. Oncogene 28:306-312. http://dx.doi.org/10.1038/onc.2008.384.

59. Coussens LM, Werb Z. 2002. Inflammation and cancer. Nature 420:860-867. http://dx.doi.org/10.1038/nature01322.

60. Rodrigue-Gervais IG, Labbe K, Dagenais M, Dupaul-Chicoine J, Champagne C, Morizot A, Skeldon A, Brincks EL, Vidal SM, Griffith TS, Saleh M. 2014. Cellular inhibitor of apoptosis protein cIAP2 protects against pulmonary tissue necrosis during influenza virus infection to promote host survival. Cell Host Microbe 15:23-35. http://dx.doi.org/10.1016/j.chom.2013.12.003.

61. Nogusa S, Thapa RJ, Dillon CP, Liedmann S, Oguin TH, 3rd, Ingram JP, Rodriguez DA, Kosoff R, Sharma S, Sturm O, Verbist K, Gough PJ, Bertin J, Hartmann BM, Sealfon SC, Kaiser WJ, Mocarski ES, Lopez CB, Thomas PG,

Oberst A, Green DR, Balachandran S. 2016. RIPK3 Activates Parallel Pathways of MLKL-Driven Necroptosis and FADD-Mediated Apoptosis to Protect against Influenza A Virus. Cell Host Microbe 20:13-24. http://dx.doi.org/10.1016/j.chom.2016.05.011.

62. Guo H, Omoto S, Harris PA, Finger JN, Bertin J, Gough PJ, Kaiser WJ, Mocarski ES. 2015. Herpes simplex virus suppresses necroptosis in human cells. Cell Host Microbe 17:243-251. http://dx.doi.org/10.1016/j.chom.2015.01.003.

63. Omoto S, Guo H, Talekar GR, Roback L, Kaiser WJ, Mocarski ES. 2015. Suppression of RIP3-dependent necroptosis by human cytomegalovirus. J Biol Chem 290:11635-11648. http://dx.doi.org/10.1074/jbc.M115.646042.

64. Gaiha GD, McKim KJ, Woods M, Pertel T, Rohrbach J, Barteneva N, Chin CR, Liu D, Soghoian DZ, Cesa K, Wilton S, Waring MT, Chicoine A, Doering T, Wherry EJ, Kaufmann DE, Lichterfeld M, Brass AL, Walker BD. 2014. Dysfunctional HIV-specific CD8+ T cell proliferation is associated with increased caspase-8 activity and mediated by necroptosis. Immunity 41:1001-1012. http://dx.doi.org/10.1016/j.immuni.2014.12.011.

65. Ichinohe T, Lee HK, Ogura Y, Flavell R, Iwasaki A. 2009. Inflammasome recognition of influenza virus is essential for adaptive immune responses. J Exp Med 206:79-87. http://dx.doi.org/10.1084/jem.20081667.

66. Thomas PG, Dash P, Aldridge JR, Jr., Ellebedy AH, Reynolds C, Funk AJ, Martin WJ, Lamkanfi M, Webby RJ, Boyd KL, Doherty PC, Kanneganti TD. 2009. The intracellular sensor NLRP3 mediates key innate and healing responses to influenza A virus via the regulation of caspase-1. Immunity 30:566-575. http://dx.doi.org/10.1016/j.immuni.2009.02.006.

67. Allen IC, Scull MA, Moore CB, Holl EK, McElvania-TeKippe E, Taxman DJ, Guthrie EH, Pickles RJ, Ting JP. 2009. The NLRP3 inflammasome mediates in vivo innate immunity to influenza A virus through recognition of viral RNA. Immunity 30:556-565. http://dx.doi.org/10.1016/j.immuni.2009.02.005.

68. Hornung V, Ablasser A, Charrel-Dennis M, Bauernfeind F, Horvath G, Caffrey DR, Latz E, Fitzgerald KA. 2009. AIM2 recognizes cytosolic dsDNA and forms a caspase-1-activating inflammasome with ASC. Nature 458:514-518. http://dx.doi.org/10.1038/nature07725.

69. Kerur N, Veettil MV, Sharma-Walia N, Bottero V, Sadagopan S, Otageri P, Chandran B. 2011. IFI16 acts as a nuclear pathogen sensor to induce the inflammasome in response to Kaposi Sarcoma-associated herpesvirus infection. Cell Host Microbe 9:363-375. http://dx.doi.org/10.1016/j.chom.2011.04.008.

70. Franchi L, Kamada N, Nakamura Y, Burberry A, Kuffa P, Suzuki S, Shaw MH, Kim YG, Nunez G. 2012. NLRC4-driven production of IL-1beta discriminates between pathogenic and commensal bacteria and promotes host intestinal defense. Nat Immunol 13:449-456. http://dx.doi.org/10.1038/ni.2263.

71. Zhu S, Ding S, Wang P, Wei Z, Pan W, Palm NW, Yang Y, Yu H, Li HB, Wang G, Lei X, de Zoete MR, Zhao J, Zheng Y, Chen H, Zhao Y, Jurado KA, Feng N, Shan L, Kluger Y, Lu J, Abraham C, Fikrig E, Greenberg HB, Flavell RA. 2017. Nlrp9b inflammasome restricts rotavirus infection in intestinal epithelial cells. Nature 546:667-670. http://dx.doi.org/10.1038/nature22967.

72. Haller O, Gao S, von der Malsburg A, Daumke O, Kochs G. 2010. Dynamin-like MxA GTPase: structural insights into oligomerization and implications

for antiviral activity. J Biol Chem 285:28419-28424. http://dx.doi.org/10.1074/jbc.R110.145839.

73. Haller O, Kochs G. 2011. Human MxA protein: an interferon-induced dynamin-like GTPase with broad antiviral activity. J Interferon Cytokine Res 31:79-87. http://dx.doi.org/10.1089/jir.2010.0076.

74. Verhelst J, Hulpiau P, Saelens X. 2013. Mx proteins: antiviral gatekeepers that restrain the uninvited. Microbiol Mol Biol Rev 77:551-566. http://dx.doi.org/10.1128/mmbr.00024-13.

75. Haller O, Stertz S, Kochs G. 2007. The Mx GTPase family of interferon-induced antiviral proteins. Microbes Infect 9:1636-1643. http://dx.doi.org/10.1016/j.micinf.2007.09.010.

76. Grimm D, Staeheli P, Hufbauer M, Koerner I, Martinez-Sobrido L, Solorzano A, Garcia-Sastre A, Haller O, Kochs G. 2007. Replication fitness determines high virulence of influenza A virus in mice carrying functional Mx1 resistance gene. Proc Natl Acad Sci U S A 104:6806-6811. http://dx.doi.org/10.1073/pnas.0701849104.

77. Tumpey TM, Szretter KJ, Van Hoeven N, Katz JM, Kochs G, Haller O, Garcia-Sastre A, Staeheli P. 2007. The Mx1 gene protects mice against the pandemic 1918 and highly lethal human H5N1 influenza viruses. J Virol 81:10818-10821. http://dx.doi.org/10.1128/jvi.01116-07.

78. Haller O, Frese M, Rost D, Nuttall PA, Kochs G. 1995. Tick-borne thogoto virus infection in mice is inhibited by the orthomyxovirus resistance gene product Mx1. J Virol 69:2596-2601.

79. Pavlovic J, Zurcher T, Haller O, Staeheli P. 1990. Resistance to influenza virus and vesicular stomatitis virus conferred by expression of human MxA protein. J Virol 64:3370-3375.

80. Pavlovic J, Arzet HA, Hefti HP, Frese M, Rost D, Ernst B, Kolb E, Staeheli P, Haller O. 1995. Enhanced virus resistance of transgenic mice expressing the human MxA protein. J Virol 69:4506-4510.

81. Kochs G, Janzen C, Hohenberg H, Haller O. 2002. Antivirally active MxA protein sequesters La Crosse virus nucleocapsid protein into perinuclear complexes. Proc Natl Acad Sci U S A 99:3153-3158. http://dx.doi.org/10.1073/pnas.052430399.

82. Chappie JS, Acharya S, Liu YW, Leonard M, Pucadyil TJ, Schmid SL. 2009. An intramolecular signaling element that modulates dynamin function in vitro and in vivo. Mol Biol Cell 20:3561-3571. http://dx.doi.org/10.1091/mbc.E09-04-0318.

83. Rennie ML, McKelvie SA, Bulloch EM, Kingston RL. 2014. Transient dimerization of human MxA promotes GTP hydrolysis, resulting in a mechanical power stroke. Structure 22:1433-1445. http://dx.doi.org/10.1016/j.str.2014.08.015.

84. Di Paolo C, Hefti HP, Meli M, Landis H, Pavlovic J. 1999. Intramolecular backfolding of the carboxyl-terminal end of MxA protein is a prerequisite for its oligomerization. J Biol Chem 274:32071-32078.

85. Gao S, von der Malsburg A, Paeschke S, Behlke J, Haller O, Kochs G, Daumke O. 2010. Structural basis of oligomerization in the stalk region of dynamin-like MxA. Nature 465:502-506. http://dx.doi.org/10.1038/nature08972.

86. Kochs G, Haener M, Aebi U, Haller O. 2002. Self-assembly of human MxA GTPase into highly ordered dynamin-like oligomers. J Biol Chem 277:14172-14176. http://dx.doi.org/10.1074/jbc.M200244200.

87. Gao S, von der Malsburg A, Dick A, Faelber K, Schroder GF, Haller O, Kochs G, Daumke O. 2011. Structure of myxovirus resistance protein a reveals intra- and intermolecular domain interactions required for the antiviral function. Immunity 35:514-525. http://dx.doi.org/10.1016/j.immuni.2011.07.012.

88. Pitossi F, Blank A, Schroder A, Schwarz A, Hussi P, Schwemmle M, Pavlovic J, Staeheli P. 1993. A functional GTP-binding motif is necessary for antiviral activity of Mx proteins. J Virol 67:6726-6732.

89. Ponten A, Sick C, Weeber M, Haller O, Kochs G. 1997. Dominant-negative mutants of human MxA protein: domains in the carboxy-terminal moiety are important for oligomerization and antiviral activity. J Virol 71:2591-2599.

90. Turan K, Mibayashi M, Sugiyama K, Saito S, Numajiri A, Nagata K. 2004. Nuclear MxA proteins form a complex with influenza virus NP and inhibit the transcription of the engineered influenza virus genome. Nucleic Acids Res 32:643-652. http://dx.doi.org/10.1093/nar/gkh192.

91. Kawaguchi A, Nagata K. 2007. De novo replication of the influenza virus RNA genome is regulated by DNA replicative helicase, MCM. Embo j 26:4566-4575. http://dx.doi.org/10.1038/sj.emboj.7601881.

92. Haruki H, Okuwaki M, Miyagishi M, Taira K, Nagata K. 2006. Involvement of template-activating factor I/SET in transcription of adenovirus early genes as a positive-acting factor. J Virol 80:794-801. http://dx.doi.org/10.1128/jvi.80.2.794-801.2006.

93. Deeg CM, Hassan E, Mutz P, Rheinemann L, Gotz V, Magar L, Schilling M, Kallfass C, Nurnberger C, Soubies S, Kochs G, Haller O, Schwemmle M, Staeheli P. 2017. In vivo evasion of MxA by avian influenza viruses requires human signature in the viral nucleoprotein. J Exp Med 214:1239-1248. http://dx.doi.org/10.1084/jem.20161033.

94. Kovarova M, Hesker PR, Jania L, Nguyen M, Snouwaert JN, Xiang Z, Lommatzsch SE, Huang MT, Ting JP, Koller BH. 2012. NLRP1-dependent pyroptosis leads to acute lung injury and morbidity in mice. J Immunol 189:2006-2016. http://dx.doi.org/10.4049/jimmunol.1201065.

95. Kuida K, Lippke JA, Ku G, Harding MW, Livingston DJ, Su MS, Flavell RA. 1995. Altered cytokine export and apoptosis in mice deficient in interleukin-1 beta converting enzyme. Science 267:2000-2003.

96. Mibayashi M, Nakad K, Nagata K. 2002. Promoted cell death of cells expressing human MxA by influenza virus infection. Microbiol Immunol 46:29-36.

97. Ichinohe T, Pang IK, Iwasaki A. 2010. Influenza virus activates inflammasomes via its intracellular M2 ion channel. Nat Immunol 11:404-410. http://dx.doi.org/10.1038/ni.1861.

98. Numajiri A, Mibayashi M, Nagata K. 2006. Stimulus-dependent and domain-dependent cell death acceleration by an IFN-inducible protein, human MxA. J Interferon Cytokine Res 26:214-219. http://dx.doi.org/10.1089/jir.2006.26.214.

99. Haller O, Staeheli P, Schwemmle M, Kochs G. 2015. Mx GTPases: dynamin-like antiviral machines of innate immunity. Trends Microbiol 23:154-163. http://dx.doi.org/10.1016/j.tim.2014.12.003.

100. He Y, Zeng MY, Yang D, Motro B, Nunez G. 2016. NEK7 is an essential mediator of NLRP3 activation downstream of potassium efflux. Nature 530:354-357. http://dx.doi.org/10.1038/nature16959.

101. Shi H, Wang Y, Li X, Zhan X, Tang M, Fina M, Su L, Pratt D, Bu CH, Hildebrand S, Lyon S, Scott L, Quan J, Sun Q, Russell J, Arnett S, Jurek P, Chen D, Kravchenko VV, Mathison JC, Moresco EM, Monson NL, Ulevitch RJ, Beutler B. 2016. NLRP3 activation and mitosis are mutually exclusive events coordinated by NEK7, a new inflammasome component. Nat Immunol 17:250-258. http://dx.doi.org/10.1038/ni.3333.

102. von der Malsburg A, Abutbul-Ionita I, Haller O, Kochs G, Danino D. 2011. Stalk domain of the dynamin-like MxA GTPase protein mediates membrane binding and liposome tubulation via the unstructured L4 loop. J Biol Chem 286:37858-37865. http://dx.doi.org/10.1074/jbc.M111.249037.

103. Staeheli P, Grob R, Meier E, Sutcliffe JG, Haller O. 1988. Influenza virus-susceptible mice carry Mx genes with a large deletion or a nonsense mutation. Mol Cell Biol 8:4518-4523.

104. Oroz J, Barrera-Vilarmau S, Alfonso C, Rivas G, de Alba E. 2016. ASC Pyrin Domain Self-associates and Binds NLRP3 Protein Using Equivalent Binding Interfaces. J Biol Chem 291:19487-19501. http://dx.doi.org/10.1074/jbc.M116.741082.